nature immunology

ARTICLES

https://doi.org/10.1038/s41590-018-0311-z

The transcription factor c-Myb regulates CD8+ T cell stemness and antitumor immunity

Sanjivan Gautam[1], Jessica Fioravanti[1], Wei Zhu[2], John B. Le Gall[1], Philip Brohawn[3], Neal E. Lacey[1], Jinhui Hu[1], James D. Hocker[1], Nga Voong Hawk[1], Veena Kapoor[1], William G. Telford[1], Devikala Gurusamy[4], Zhiya Yu[4], Avinash Bhandoola[5], Hai-Hui Xue[6], Rahul Roychoudhuri[7], Brandon W. Higgs[3], Nicholas P. Restifo[4], Timothy P. Bender[8,9], Yun Ji[1,10] and Luca Gattinoni[1*]

Stem cells are maintained by transcriptional programs that promote self-renewal and repress differentiation. Here, we found that the transcription factor c-Myb was essential for generating and maintaining stem cells in the CD8+ T cell memory compartment. Following viral infection, CD8+ T cells lacking *Myb* underwent terminal differentiation and generated fewer stem cell–like central memory cells than did *Myb*-sufficient T cells. c-Myb acted both as a transcriptional activator of *Tcf7* (which encodes the transcription factor Tcf1) to enhance memory development and as a repressor of *Zeb2* (which encodes the transcription factor Zeb2) to hinder effector differentiation. Domain-mutagenesis experiments revealed that the transactivation domain of c-Myb was necessary for restraining differentiation, whereas its negative regulatory domain was critical for cell survival. *Myb* overexpression enhanced CD8+ T cell memory formation, polyfunctionality and recall responses that promoted curative antitumor immunity after adoptive transfer. These findings identify c-Myb as a pivotal regulator of CD8+ T cell stemness and highlight its therapeutic potential.

Tissue homeostasis relies on the activity of a small population of adult stem cells that have the capacity to generate short-lived differentiated cells while maintaining their identity through self-renewal[1]. Recently, in vivo clonogenic studies have revealed that in the mature T cell compartment, adult stem cells are confined to the CD62L+ memory T cell pool (which comprises stem cell–like memory T cells and central memory T cells (T_{CM} cells))[2–4]. There has been growing interest in the identification of the molecular, epigenetic and metabolic factors orchestrating the formation and maintenance of stem cell–like T cells, since these cells are known to be critical for the long-term efficacy of T cell–based immunotherapy and vaccines[5].

It has become increasingly clear that several transcriptional networks regulating stem cell behavior are also used by T cells to promote the development and maintenance of stem cell–like memory cells and to restrain terminal effector differentiation[5,6]. For instance, Forkhead box protein O1 (Foxo1), T cell factor 1 (Tcf1), signal transducer and activator of transcription 3 (STAT3) and the DNA-binding-protein inhibitor Id3, which are essential for embryonic stem cell homeostasis and pluripotency[7–10], have been shown to regulate T cell stemness and the formation of memory T cells[11–16].

The gene encoding the transcription factor c-Myb has higher expression in human stem cell–like memory CD8+ T cells than in either naïve cells or effector memory cells[17]. In mouse models, c-Myb regulates thymocyte development[18] and regulatory T cell effector differentiation[19], but its function in CD8+ T cells is unknown. Given the critical role of c-Myb in the regulation of stem cells and progenitor cells in diverse tissues, including the bone marrow, colonic crypts and neurogenic regions of the brain[20,21], we hypothesized that it also plays a pivotal role in the regulation of stem cell–like behavior in T cells.

Here, we determine that c-Myb is a critical regulator of CD8+ T cell stemness. c-Myb promoted pro-memory and survival programs via the induction of *Tcf7* (which encodes Tcf1) and *Bcl2* (which encodes the anti-apoptotic protein Bcl2) and limited effector differentiation through the repression of *Zeb2* (which encodes Zeb2). We further show that while the c-Myb transactivation domain (TAD) is pivotal for restraining CD8+ T cell differentiation, the negative regulatory domain (NRD) mediated cell-survival processes. Finally, we demonstrate that the activity of c-Myb can be therapeutically harnessed to enhance the formation of stem cell–like T_{CM} cells and promote curative antitumor immunity in a melanoma model of adoptive immunotherapy.

Results

c-Myb promotes the formation of stem cell–like T_{CM} cells by restraining terminal differentiation. To evaluate the role of c-Myb in T cell differentiation, we employed pmel-1 CD8+ T cells (which recognize the shared melanoma–melanocyte differentiation antigen gp100)[22] carrying *lox*P-flanked alleles encoding c-Myb ($Myb^{fl/fl}$). Because c-Myb plays critical roles during thymocyte development[18], we bred a conditional knockout model based on a tamoxifen-regulated form of Cre ($Cre\text{-}ER^{T2}$)[23], pmel-1 $cre\text{-}ER^{T2}$ $Myb^{fl/fl}$, to acutely delete *Myb* in mature CD8+ T cells (Fig. 1a). Naive pmel-1 $Myb^{\Delta/\Delta}$ or

[1]Experimental Transplantation and Immunology Branch, Center for Cancer Research, National Cancer Institute, Bethesda, MD, USA. [2]Department of Bioinformatics, Inova Translational Medicine Institute, Fairfax, VA, USA. [3] MedImmune , Gaithersburg, MD, USA. [4]Surgery Branch, Center for Cancer Research, National Cancer Institute, Bethesda, MD, USA. [5]Laboratory of Genome Integrity, Center for Cancer Research, National Cancer Institute, Bethesda, MD, USA. [6]Department of Microbiology, Carver College of Medicine, University of Iowa, Iowa City, IA, USA. [7]Laboratory of Lymphocyte Signaling and Development, Babraham Institute, Cambridge, UK. [8]Department of Microbiology, University of Virginia, Charlottesville, VA, USA. [9]Beirne B. Carter Center for Immunology Research, University of Virginia, Charlottesville, VA, USA. [10]Present address: Cellular Biomedicine Group, Gaithersburg, MD, USA. *e-mail: gattinol@mail.nih.gov

pmel-1 *Myb*$^{fl/fl}$ T cells isolated from littermates (Fig. 1b) were adoptively transferred into wild-type mice infected with a recombinant strain of vaccinia virus encoding gp100 (gp100-VV), and antigen-specific CD8$^+$ T cell expansion and persistence were monitored over time (Fig. 1c). We found that in the absence of *Myb*, CD8$^+$ T cells showed a minor defect in splenic accumulation during the acute phase of the immune response (Fig. 1d,e). However, following the peak of expansion, the number of c-Myb-deficient T cells contracted more sharply than did that of wild-type cells, resulting in fewer memory cells 1 month after transfer. A steep decline in c-Myb-deficient CD8$^+$ T cell frequency during the contraction phase was similarly observed in lymph nodes (Supplementary Fig. 1a,b) and lungs (Supplementary Fig. 1c,d), underscoring the importance of c-Myb in cell maintenance.

To determine whether the reduced accumulation of c-Myb-deficient CD8$^+$ T cells was due to defects in proliferation, we measured 5-bromo-2′-deoxyuridine (BrdU) uptake in transferred cells responding to gp100-VV infection. Early on, most antigen-specific cells were vigorously proliferating, independently of the presence of c-Myb (Supplementary Fig. 2a,b). Surprisingly, a substantial fraction of c-Myb-deficient T cells continued to take up BrdU, while most wild-type CD8$^+$ T cells stopped actively dividing at the peak of expansion (Supplementary Fig. 2a,b). Thus, the reduced accumulation of *Myb*$^{\Delta/\Delta}$ T cells was not caused by defective proliferation. Therefore, we determined whether the differences in cell numbers were linked to a survival disadvantage. Measuring apoptosis with annexin V revealed that in the absence of *Myb*, CD8$^+$ T cells underwent massive apoptosis in the initial phase of the immune response (Supplementary Fig. 2c,d). This tendency, although not statistically significant, was also observed at the peak of the response (Supplementary Fig. 2c,d). These data emphasize the pivotal role of c-Myb in mature T cell survival, consistent with known findings in thymocytes[18,24].

Increased turnover and apoptosis of pmel-1 *Myb*$^{\Delta/\Delta}$ T cells might result from alteration of their differentiation program. We therefore evaluated the frequency of memory precursors and terminally differentiated effector T cells (T_{TE} cells) by measuring the expression of KLRG1 and CD62L on transferred pmel-1 T cells 5 d after gp100-VV infection. The deletion of *Myb* resulted in a four-fold increase in splenic KLRG1$^+$CD62L$^-$ T_{TE} cells and a dramatic loss of KLRG1$^-$CD62L$^+$ memory precursors, compared to controls (Fig. 1f,g). Similarly, there was a marked accumulation of T_{TE} cells and depletion of CD62L$^+$ cells among c-Myb-deficient T cells in the lymph nodes and lungs (Supplementary Fig. 3). These findings were also observed when physiological numbers of antigen-specific T cells[25] were transferred (data not shown). Although we did not measure major differences in perforin expression (data not shown), *Myb*-deficient T cells displayed a larger amount of granzyme B (Fig. 1h) and enhanced killing capacity in vitro (Fig. 1i), in further support of the observation that c-Myb inhibits terminal effector differentiation. As T cells progressively differentiate into T_{TE} cells, they first lose the capacity to produce interleukin 2 (IL-2) and then the capacity to produce tumor necrosis factor (TNF) before ultimately becoming monofunctional interferon-γ (IFN-γ) producers[26]. *Myb*$^{\Delta/\Delta}$ T cells exhibited poor polyfunctionality, as evidenced by the reduced frequency of IL-2$^+$TNF$^+$ IFN-γ$^+$ cells (Fig. 1j,k). Notably, nearly half of the cytokine-producing *Myb*$^{\Delta/\Delta}$ T cells were single IFN-γ producers, functionally consistent with our observation that CD8$^+$ T cells were driven toward terminal differentiation in the absence of c-Myb. T cell differentiation is also intrinsically linked to changes in metabolism. For instance, effector T cells display reduced oxidative metabolism and mitochondrial spare respiratory capacity (SRC) compared with that of memory cells[27]. Accordingly, *Myb*$^{\Delta/\Delta}$ T cells displayed a lower basal oxygen-consumption rate (OCR) and a striking reduction in SRC compared with that of wild-type cells (Fig. 1l–n). These differences in cellular metabolism were in part independent of a skewed T_{TE} cell frequency, as manifested by a small but significant reduction of mitochondrial fatty acid oxidation in *Myb*-deficient T cells after phenotypic normalization (Supplementary Fig. 4). Taken together, phenotypic, functional and metabolic analyses concordantly demonstrate that c-Myb restrains CD8$^+$ T cell terminal differentiation.

Consistent with a reduction in memory precursors generated in the acute phase of the immune response, we observed both decreased quantities of total memory cells (Fig. 1d,e) and decreased frequencies of stem cell–like T_{CM} cells in *Myb*-deficient T cells 30 d after transfer (Fig. 1o,p). The hallmark function of memory cells is the ability to mount a robust response after secondary infection. To determine whether *Myb*-deficient memory T cells were functionally competent, we transferred equal numbers of *Myb*$^{\Delta/\Delta}$ or wild-type memory T cells into syngeneic hosts and measured their expansion 5 d after infection with gp100-encoding adenovirus type 2 (gp100-Adv). Strikingly, we observed a dramatic impairment in the ability of *Myb*$^{\Delta/\Delta}$ T cells to mount secondary immune responses (Fig. 1q,r). Together, these results demonstrate that c-Myb is essential for the generation of long-lived and functional stem cell–like T_{CM} cells.

c-Myb is indispensable for CD8$^+$ T cell stemness. Persistence is a hallmark of stemness[4]. To determine the role of c-Myb in the persistence of CD8$^+$ T cells, we first evaluated the long-term maintenance of memory cells generated in the absence of *Myb* by measuring the frequency and number of adoptively transferred pmel-1

Fig. 1 | c-Myb promotes the formation of stem cell–like T_{CM} cells by restraining terminal differentiation. a, Immunoblot showing c-Myb in naïve CD8$^+$ T cells from pmel-1 *Myb*$^{fl/fl}$ *Cre- ER*^{T2} mice 5 d after intraperitoneal treatment with tamoxifen or vehicle. GAPDH served as control. **b**, Flow cytometry of pmel-1 *Myb*$^{fl/fl}$ and *Myb*$^{\Delta/\Delta}$ CD8$^+$ T cells after naïve T cell enrichment. **c**, Experimental design testing c-Myb's impact on pmel-1 CD8$^+$ T cell primary and secondary immune responses. **d**,**e**, Flow cytometry of splenic CD8$^+$ T cells (**d**) and numbers of pmel-1 T cells (**e**), after transfer of 10^5 pmel-1 Thy1.1$^+$ *Myb*$^{fl/fl}$ or pmel-1 Thy1.1$^+$ *Myb*$^{\Delta/\Delta}$ CD8$^+$ T cells into wild-type mice infected with gp100-VV, assessed 0–30 d after infection ($n = 3$ mice per group per time point). **f**, Flow cytometry of pmel-1 T cells 5 d after transfer as in **d**,**e**. **g**, Percentages (left) and numbers (right) of CD62L$^-$ KLRG1$^+$ and CD62L$^+$ KLRG1$^-$ pmel-1 T cells 5 d after transfer as in **d**,**e**. **h**, Flow cytometry (left) and geometric mean fluorescence intensity (gMFI) (right) of pmel-1 T cells 5 d after transfer as in **d**. **i**, Cell index (top) and percentage of lysis (bottom) of B16-hgp100 melanoma after co-culture with pmel-1 *Myb*$^{+/+}$ or pmel-1 *Myb*$^{\Delta/\Delta}$ CD8$^+$ T cells ($n = 6$ technical replicates). **j**,**k**, Intracellular cytokine staining (**j**) and combinatorial cytokine production (**k**) by pmel-1 T cells 5 d after transfer as in **d**,**e**. **l**, OCR of pmel-1 *Myb*$^{+/+}$ and pmel-1 *Myb*$^{\Delta/\Delta}$ CD8$^+$ T cells activated in vitro with antibodies to CD3 and CD28 in the presence of IL-2. Data shown were obtained under basal conditions and in response to the indicated molecules ($n = 5$ technical replicates). FCCP, carbonyl cyanide 4-(trifluoromethoxy)phenylhydrazone; Ant, antimycin; Rot, rotenone. **m**,**n**, Basal OCR (**m**) and SRC (**n**) of pmel-1 T cells generated as in **l** ($n = 15$ technical replicates; five replicates × three time points). **o**, Flow cytometry of pmel-1 T cells in the lymph nodes 30 d after transfer as in **d**,**e**. **p**, Percentage of KLRG1$^-$CD62L$^+$ pmel-1 T cells in the lymph nodes 30 d after transfer as in **d**,**e**. **q**,**r**, Flow cytometry of splenocytes (**q**) and numbers of splenic pmel-1 T cells (**r**) 5 d after the transfer of 5×10^4 pmel-1 Ly5.2$^+$ *Myb*$^{fl/fl}$ or pmel-1 Ly5.2$^+$ *Myb*$^{\Delta/\Delta}$ primary memory CD8$^+$ T cells, followed by secondary infection with gp100-adV ($n = 3$). Data are representative of at least two independent experiments. Data are shown after gating on live CD8$^+$ cells (**b**,**d**), CD8$^+$ Thy1.1$^+$ cells (**f**,**h**,**j**,**o**) or CD8$^+$ Ly5.2$^+$ cells (**q**). Data in **e**–**j**,**l**–**n**,**p**,**r** are shown as mean ± s.e.m.; each symbol represents an individual mouse (**g**,**h**,**p**,**r**) or technical replicate (**i**,**m**,**n**). NS, not significant; $^*P < 0.05$, $^{**}P < 0.01$, $^{***}P < 0.001$ and $^{****}P < 0.0001$, (unpaired two-tailed Student's *t*-test).

Myb$^{\Delta/\Delta}$ or pmel-1 *Myb*$^{fl/fl}$ T cells 90 d after infection with gp100-VV (Fig. 2a). Notably, we found a striking reduction in the number of total and stem cell–like T_{CM} cells in the spleen of mice that received *Myb*-deficient cells, compared with that of controls (Fig. 2b,c). The reduction in the number of *Myb*$^{\Delta/\Delta}$ T cells was not due to a skewed distribution, because *Myb*$^{\Delta/\Delta}$ T cells were similarly decreased in lungs and lymph nodes (Supplementary Fig. 5a–d). Compared to results obtained at day 30 (Fig. 1d,e), we observed wider differences in cell frequencies and numbers, indicating that memory cells undergo progressive attrition in the absence of c-Myb.

Second, we determined the ability of *Myb*-deficient T cells to generate secondary memory cells. We transferred equal numbers of memory cells generated 45 d after primary infection into secondary recipients and assessed the frequency and number of pmel-1

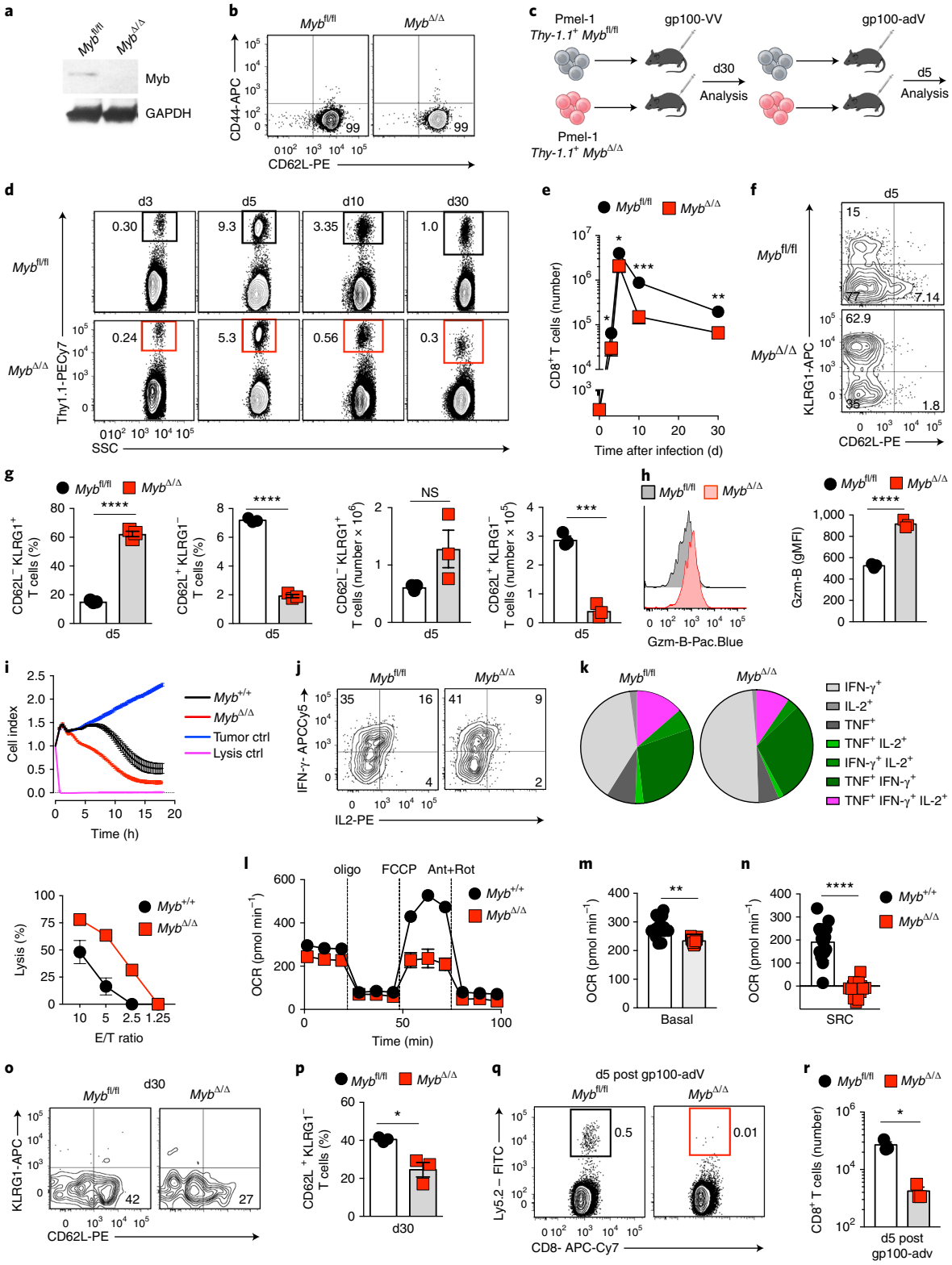

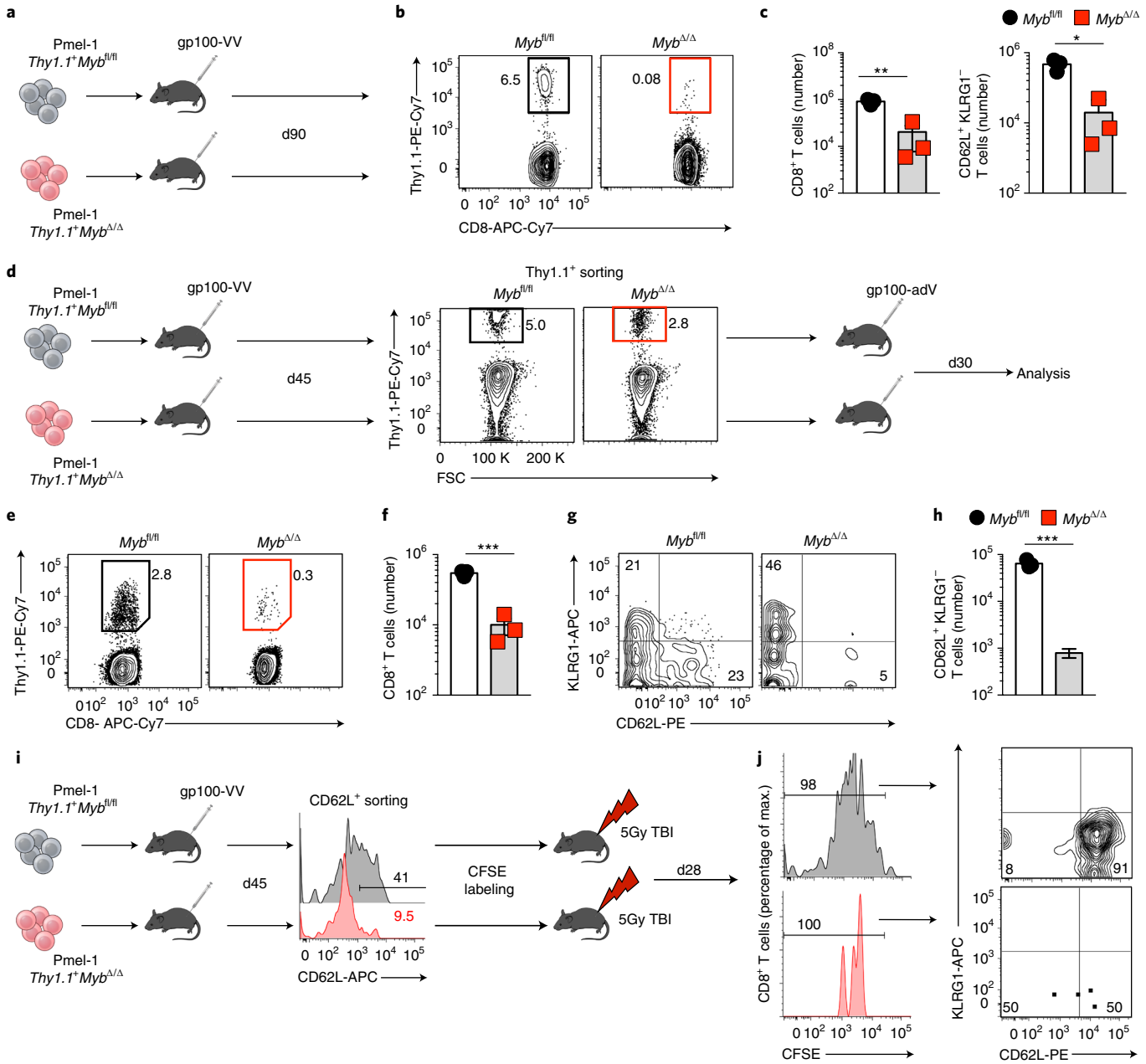

Fig. 2 | c-Myb is indispensable for CD8⁺ T cell stemness. a, Experimental design assessing c-Myb function in long-term memory. **b**, Flow cytometry of splenic CD8⁺ T cells after transfer of 3×10^5 pmel-1 Thy1.1⁺ *Myb*$^{fl/fl}$ or pmel-1 Thy1.1⁺ *Myb*$^{\Delta/\Delta}$ CD8⁺ T cells into wild-type mice infected with gp100-VV, assessed 90 d after infection ($n=3$ mice per group). **c**, Numbers of total (left) and CD62L⁺ KLRG1⁻ (right) pmel-1 T cells after transfer as in **b**. **d**, Experimental design testing c-Myb's impact on secondary memory. Middle, flow cytometry exemplifying Thy1.1⁺ T cell frequencies 45 d after transfer as in **b**. **e**,**f**, Flow cytometry of splenocytes (**e**) and numbers of splenic pmel-1 Thy1.1⁺ CD8⁺ T cells (**f**) after transfer of 5×10^4 primary memory pmel-1 Thy1.1⁺ *Myb*$^{fl/fl}$ or pmel-1 Thy1.1⁺ *Myb*$^{\Delta/\Delta}$ CD8⁺ T cells, assessed 30 d after gp100-adV infection ($n=3$ mice per group). **g**, Flow cytometry of splenic pmel-1 T cells 30 d after transfer as in **e**,**f**. **h**, Numbers of splenic CD62L⁺ KLRG1⁻ pmel-1 T cells obtained as in **g**. **i**, Experimental design evaluating the self-renewal of stem cell–like T_{CM} cells. Middle, flow cytometry exemplifying the sorting strategy for the isolation of CD62L⁺ pmel-1 memory T cells from spleens and lymph nodes 45 d after transfer of 10^6 pmel-1 Thy1.1⁺ *Myb*$^{fl/fl}$ or pmel-1 Thy1.1⁺ *Myb*$^{\Delta/\Delta}$ CD8⁺ T cells into wild-type mice infected with gp100-VV. **j**, Flow cytometry of pmel-1 Thy1.1⁺ CD8⁺ T cells 28 d after transfer of 10^5 CFSE-labeled CD62L⁺ pmel-1 Thy1.1⁺ *Myb*$^{fl/fl}$ or pmel-1 Thy1.1⁺ *Myb*$^{\Delta/\Delta}$ CD8⁺ T cells into sub-lethally irradiated mice ($n=2$ mice per group, data shown after concatenation). Data are shown after gating on live cells (**e**) live CD8⁺ cells (**b**, **d**) or live CD8⁺ Thy1.1⁺ cells (**g**, **j**). Data in **c**,**f**,**h** are shown as mean ± s.e.m.; each symbol represents an individual mouse (**c**,**f**,**h**). $^*P<0.05$, $^{**}P<0.01$ and $^{***}P<0.001$ (unpaired two-tailed Student's *t*-test).

Myb$^{\Delta/\Delta}$ or pmel-1 *Myb*$^{fl/fl}$ T cells 1 month after infection with gp100-Adv (Fig. 2d). *Myb*-deficient T cells exhibited a reduced capacity to form secondary memory cells in all organs evaluated (Fig. 2e,f and Supplementary Fig. 5e–h). More importantly, the generation of stem cell–like T_{CM} cells was markedly impaired, as evidenced by a 98.8% reduction in splenic CD62L⁺ T cell numbers (Fig. 2g,h).

Finally, we tested the impact of *Myb* deficiency on stem cell–like T_{CM} cell self-renewal. We labeled flow cytometry–sorted CD62L⁺ memory CD8⁺ T cells with the division-tracking dye CFSE (carboxyfluorescein succinimidyl ester) and transferred them into sub-lethally irradiated mice (Fig. 2i). 4 weeks later, we measured CFSE dilution and maintenance of a stem cell–like phenotype under

homeostatic proliferation. Wild-type T cells displayed robust self-renewal, as shown by the retention of CD62L expression on CFSE-diluted cells (Fig. 2j). *Myb*-deficient T cells were unable to persist (Fig. 2j). Of note, only half of the few surviving cells were able to maintain their stem cell–like phenotype (Fig. 2j). Taken together, these experiments indicate that c-Myb is an essential regulator of CD8$^+$ T cell stemness.

c-Myb enhances CD8$^+$ T cell stemness by regulating *Tcf7*, *Bcl2* and *Zeb2* expression. To understand the mechanisms by which c-Myb regulates CD8$^+$ T cell differentiation, we performed RNA-seq of pmel-1 *Myb*$^{+/+}$ and pmel-1 *Myb*$^{\Delta/\Delta}$ T cells harvested 5 d after adoptive transfer into mice infected with gp100-VV. To minimize skewing in gene expression due to differences in T cell subset distribution among *Myb*$^{+/+}$ and *Myb*$^{\Delta/\Delta}$ T cells, we analyzed KLRG1$^-$CD62L$^-$ cells sorted with a purity of >99% by flow cytometry (Supplementary Fig. 6a). Even after subset normalization, *Myb*$^{\Delta/\Delta}$ T cells were enriched with genes known to be highly expressed in effector cells, whereas *Myb*$^{+/+}$ T cells contained a larger proportion of transcripts associated with memory precursors (Fig. 3a, Supplementary Fig. 6b,c and Supplementary Table 1). To elucidate downstream effectors of c-Myb, we filtered the dataset by selecting genes reported to be directly regulated (activated or repressed) by c-Myb in promyelocytes[28]. *Bcl2*, a well-established target of c-Myb[29,30], was downregulated in *Myb*$^{\Delta/\Delta}$ T cells (Fig. 3a and Supplementary Table 1), in keeping with the survival defect observed in pmel-1 *Myb*$^{\Delta/\Delta}$ T cells (Supplementary Fig 2c,d). Pathway analysis further revealed induction of transcriptional networks promoting cell death among *Myb*$^{\Delta/\Delta}$ T cells (Supplementary Table 2). Two genes encoding crucial transcription factors that regulate CD8$^+$ T cell differentiation, *Tcf7* and *Zeb2*[13,14,31,32], were differentially expressed in *Myb*$^{\Delta/\Delta}$ and *Myb*$^{+/+}$ cells (Fig. 3a and Supplementary Table 1). The gene encoding Tcf1 (*Tcf7*), which enhances the formation and maintenance of memory T cells, was downregulated in *Myb*$^{\Delta/\Delta}$ T cells. Conversely, *Zeb2*, which encodes a driver of CD8$^+$ T cell terminal differentiation[31,32], was upregulated in the absence of *Myb* (Fig. 3a). Gene-set–enrichment analysis (GSEA) corroborated these findings by revealing that *Myb*$^{\Delta/\Delta}$ T cells were enriched with genes upregulated in CD8$^+$ T cells lacking WNT-reporter activity[33] (Fig. 3b, left) and genes upregulated in *Zeb2*-sufficient CD8$^+$ T cells[32] (Fig. 3b, right).

To further elucidate the relationship of *Myb* expression with that of *Bcl2*, *Tcf7* and *Zeb2* during CD8$^+$ T cell differentiation, we quantified the transcripts of these genes in naïve, CD62L$^+$ and CD62L$^-$ pmel-1 T cells generated in response to gp100-VV. As *Myb* expression declined with differentiation from naïve T cells into CD62L$^-$ cells, *Bcl2* and *Tcf7* transcripts decreased (Fig. 3c,d), whereas *Zeb2* expression was inversely related to *Myb* expression (Fig. 3e). We next sought to evaluate how the genetic manipulation of *Myb* would affect *Bcl2*, *Tcf7* and *Zeb2* expression. To this end, we adoptively transferred into gp100-VV-infected mice pmel-1 *Myb*$^{+/+}$, pmel-1 *Myb*$^{\Delta/\Delta}$ and pmel-1 T cells transduced with *Myb*-Thy1.1 or Thy1.1 alone. 5 d later, we analyzed *Bcl2*, *Tcf7* and *Zeb2* expression in the transferred T cells. Reinforcing our RNA-seq results, *Myb* deletion resulted in a significant reduction in the expression of *Bcl2* and *Tcf7* (Fig. 3f,g) while dramatically increasing *Zeb2* expression (Fig. 3h). By contrast, *Myb* overexpression enhanced the expression of both *Bcl2* and *Tcf7* (Fig. 3f,g) and suppressed *Zeb2* expression (Fig. 3h). Similar findings were obtained by measurement of Bcl2 and Tcf1 proteins (Fig. 3i,j). The lack of working mouse Zeb2–specific antibodies prevented assessment of the impact of c-Myb on Zeb2 protein expression. Transcriptional regulation of *Tcf7* by c-Myb was confirmed by a reporter assay using CD8$^+$ T cells from *Tcf7*$^{GFP/+}$ mice (data not shown). *Bcl2* is regulated by c-Myb[30]. Whether c-Myb directly binds to and regulates the expression of *Tcf7* and *Zeb2* in CD8$^+$ T cells merited further analysis. We performed chromatin immunoprecipitation (ChIP) followed by qPCR in pmel-1 *Myb*$^{+/+}$ and *Myb*$^{\Delta/\Delta}$ T cells and found specific enrichment of *Tcf7* enhancer and *Zeb2* promoter regions with c-Myb immunoprecipitation in wild-type cells but not in *Myb*$^{\Delta/\Delta}$ T cells (Fig. 3k). Taken together, these findings place c-Myb as a transcriptional activator of *Bcl2* and *Tcf7* and as a transcriptional repressor of *Zeb2* in CD8$^+$ T cells.

We next sought to determine whether the tendency for *Myb*$^{\Delta/\Delta}$ CD8$^+$ T cells to undergo terminal differentiation depends on insufficient levels of *Tcf7* and unrestrained expression of *Zeb2*. To this end, we adoptively transferred pmel-1 *Myb*$^{\Delta/\Delta}$ T cells and pmel-1 *Myb*$^{\Delta/\Delta}$ *Zeb2*$^{+/\Delta}$ T cells transduced with either *Tcf7-GFP* or *GFP* alone in gp100-VV infected mice and evaluated the formation of KLRG1$^+$CD62L$^-$ T_{TE} cells in comparison with that of pmel-1 *Myb*$^{fl/fl}$ cells transduced with the *GFP* control. Testing of complete *Zeb2* deficiency on pmel-1 *Myb*$^{\Delta/\Delta}$ T cells was not possible. The *Zeb2* locus is located on chromosome 2, just 12 centimorgans from the insertion site of the pmel-1 *Tcra* and *Tcrb* transgenes[22]; therefore, there is a slim probability of obtaining a *Zeb2*$^{fl/fl}$ with pmel-1 background. Consistent with our results using naïve CD8$^+$ T cells (Fig. 1f,g), in vitro–activated pmel-1 cells engineered to express GFP alone generated higher frequencies of T_{TE} cells in the absence of *Myb* (Fig. 3l,m). Individually, overexpression of *Tcf7* or *Zeb2* haploinsufficiency significantly reduced the frequency of T_{TE} cells among pmel-1 *Myb*$^{\Delta/\Delta}$ *GFP* T cells, although *Zeb2* depletion had a more pronounced effect (Fig. 3l,m). The combination of both genetic approaches completely rescued the skewed differentiation pattern of pmel-1 *Myb*$^{\Delta/\Delta}$

Fig. 3 | c-Myb enhances CD8$^+$ T cell stemness by regulating *Tcf7*, *Bcl2* and *Zeb2* expression. a, Volcano plot showing changes in gene expression between pmel-1 *Myb*$^{+/+}$ and pmel-1 *Myb*$^{\Delta/\Delta}$ T cells. Gene expression was evaluated by RNA-seq of pmel-1 KLRG1$^-$CD62L$^-$ T cells isolated 5 d after transfer of 3×10^5 pmel-1 Thy1.1$^+$ *Myb*$^{+/+}$ and pmel-1 Thy1.1$^+$ *Myb*$^{\Delta/\Delta}$ CD8$^+$ T cells into wild-type mice infected with gp100-VV ($n=3$, each from two pooled mice per group). Triangles and squares represent genes enriched in central memory (T_{CM}) and terminal effector (T_{TE}) T cells[57], respectively. Red and blue represent genes activated and repressed by c-Myb in promyelocytes, respectively[28]. **b**, GSEA showing positive enrichment of genes upregulated in cells lacking Wnt signaling[33] (left) and in *Zeb2*-sufficient cells[32] (right) in pmel-1 *Myb*$^{\Delta/\Delta}$ T cells obtained as in **a**. **c**–**e**, Quantitative RT-PCR of *Bcl2* (**c**), *Tcf7* (**d**) and *Zeb2* (**e**) mRNA in comparison to *Myb* in naïve, CD62L$^+$ and CD62L$^-$ pmel-1 T cells sorted 5 d after transfer of 10^5 pmel-1 *Myb*$^{+/+}$ CD8$^+$ T cells as in **a**. Results are relative to *Rpl13* (*Bcl2*, *Tcf7* and *Zeb2*) or *Actb* (*Myb*) ($n=3$ technical replicates). **f**–**h**, Quantitative RT-PCR of *Bcl2* (**f**), *Tcf7* (**g**) and *Zeb2* (**h**) mRNA in pmel-1 CD62L$^+$ T cells sorted 5 d after transfer of 10^5 pmel-1 Thy1.1$^+$ *Myb*$^{+/+}$ cells, pmel-1 Thy1.1$^+$ *Myb*$^{\Delta/\Delta}$ cells or pmel-1 Thy1.2$^+$ cells engineered with *Myb*-Thy1.1 or Thy1.1 as in **a**. Results are relative to *Rpl13* ($n=3$ technical replicates). **i**,**j**, Flow cytometry of pmel-1 T cells 5 d after transfer of 10^5 pmel-1 Thy1.1$^+$ *Myb*$^{+/+}$ and pmel-1 Thy1.1$^+$ *Myb*$^{\Delta/\Delta}$ cells as in **a**. Numbers indicate gMFI ± s.e.m. ($n=3$ mice per group). **k**, ChIP-qPCR of in vitro–activated pmel-1 *Myb*$^{+/+}$ or pmel-1 *Myb*$^{\Delta/\Delta}$ CD8$^+$ T cells. Chromatin was precipitated with antibody to c-Myb or IgG and was amplified with primers specific to *Tcf7* enhancer and *Zeb2* promoter regions ($n=3$ technical replicates). **l**,**n** Flow cytometry of splenic pmel-1 T cells (**l**) and CD8$^+$ T cells (**n**) after transfer of 10^5 pmel-1 *Myb*$^{fl/fl}$, pmel-1 *Myb*$^{\Delta/\Delta}$ or pmel-1 *Myb*$^{\Delta/\Delta}$ *Zeb2*$^{+/\Delta}$ CD8$^+$ T cells transduced with pMI-GFP or pMI-GFP-*Tcf7* 10 d after transfer into wild-type mice infected with gp100-VV. **m**,**o** Percentage of KLRG1$^+$CD62L$^-$GFP$^+$CD8$^+$ T cells (**m**) and CD8$^+$ GFP$^+$ T cells (**o**) 10 d after transfer as in **l**. Data are representative of two independent experiments. Data are shown after gating on live CD8$^+$ Thy1.1$^+$ cells (**i**,**j**), live CD8$^+$ GFP$^+$ cells (**l**) or live CD8$^+$ cells (**n**). Data in **c**–**h**,**k**,**m**,**o** are mean ± s.e.m.; each symbol represents an individual mouse (**m**,**o**) or technical replicate (**c**–**h**,**k**). **m**, merged data from two independent experiments. $^*P<0.05$, $^{**}P<0.01$, $^{***}P<0.001$ and $^{****}P<0.0001$ (unpaired two-tailed Student's *t*-test).

GFP T cells (Fig. 3l,m). Despite correcting the differentiation program, these genetic maneuvers did not rescue the survival defects of pmel-1 $Myb^{\Delta/\Delta}$ T cells, implicating *Bcl2* and other downstream factors behind the pro-survival function of c-Myb (Fig. 3n,o). Thus, c-Myb promotes $CD8^+$ T cell stemness both by inducing pro-memory and survival programs via *Tcf7* and *Bcl2* and by restraining effector differentiation through suppression of *Zeb2*.

Distinct functions of c-Myb domains in the regulation of $CD8^+$ T cell differentiation and survival. To further characterize the molecular mechanisms by which c-Myb regulates $CD8^+$ T cell differentiation and survival, we generated a complement of c-Myb mutants and tested their ability to rescue the phenotype of pmel-1 $Myb^{\Delta/\Delta}$ T cells. We compared the activity of full-length c-Myb with that of three different c-Myb mutants[34]: truncated c-Myb lacking the NRD (the '*Myb* (1–330)' construct); a c-Myb mutant with a non-functional TAD (insertion of glycine and proline after the amino acid residue at position 304 (the '*Myb* 304GP' construct); and truncated c-Myb comprising the DNA-binding domain only (the '*Myb* pBind' construct) (Fig. 4a). These were cloned into an MSGV-Thy1.1

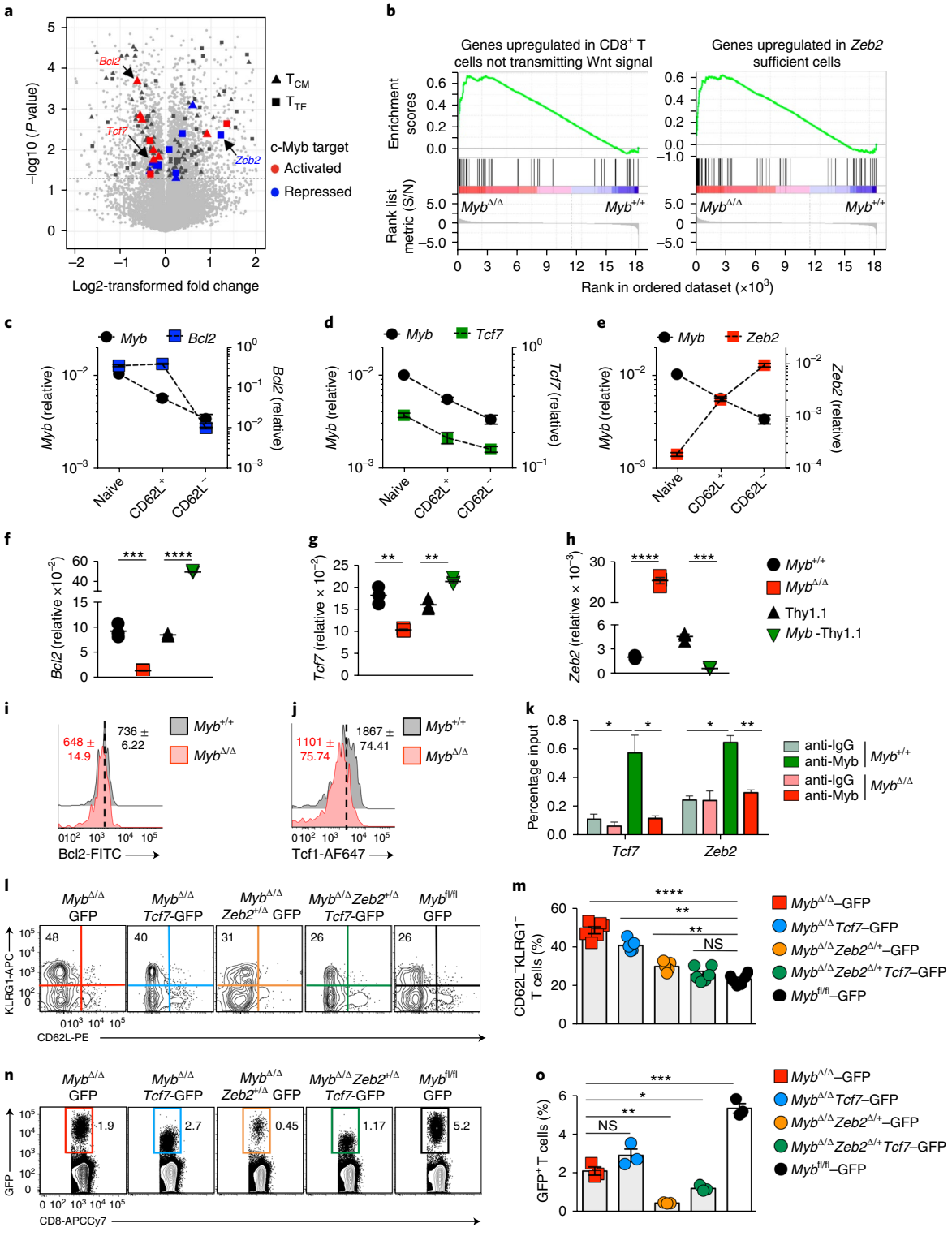

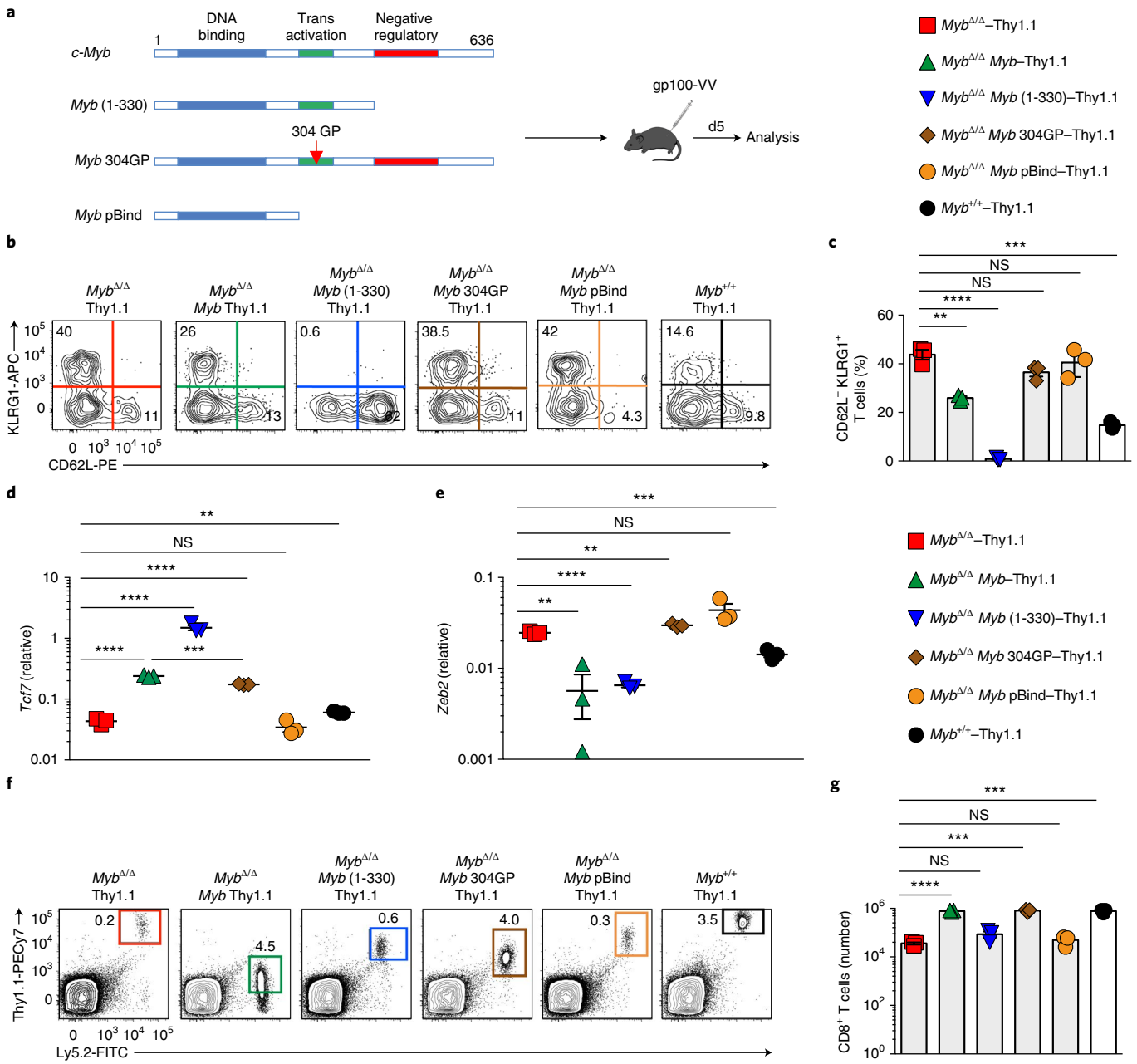

Fig. 4 | Distinct functions of c-Myb domains in the regulation of CD8⁺ T cell differentiation and survival. a, Truncated and mutant versions of c-Myb employed for complementation studies. **b**, Flow cytometry of splenic pmel-1 Thy1.1⁺ CD8⁺ T cells 5 d after transfer of 10^5 pmel-1 $Myb^{\Delta/\Delta}$ CD8⁺ T cells, transduced with MSGV-Thy1.1 encoding wild-type or mutant c-Myb, into Ly5.1⁺ mice infected with gp100-VV. pmel-1 $Myb^{+/+}$ and pmel-1 $Myb^{\Delta/\Delta}$ CD8⁺ T cells transduced with Thy1.1 served as control ($n = 3$ mice per group). **c**, Percentage of KLRG1⁺ CD62L⁻ pmel-1 T cells 5 d after transfer as in **b**. **d**,**e**, qRT-PCR of *Tcf7* (**d**) and *Zeb2* (**e**) mRNA in pmel-1 T cells sorted 5 d after transfer as in **b**. Results are relative to *Rpl13* ($n = 3$ technical replicates). **f**, Flow cytometry of CD8⁺ T cells 5 d after transfer as described in **b**. **g**, Percentage of splenic CD8⁺ Thy1.1⁺ T cells 5 d after transfer as described in **b**. Data are representative of at least two independent experiments. Data are shown after gating on live CD8⁺ Thy1.1⁺ cells (**b**) or live CD8⁺ cells (**f**). Data in **c**–**e**, and **g** are shown as the mean ± s.e.m.; shapes represent individual mice (**c**,**g**) or technical replicates (**d**,**e**). $^{**}P < 0.01$, $^{***}P < 0.001$ and $^{****}P < 0.0001$ (unpaired two-tailed Student's *t*-test).

retroviral vector to allow the sorting and tracking of transduced pmel-1 T cells after adoptive transfer into wild-type mice infected with gp100-VV (Fig. 4a). With the exception of the *Myb* pBind construct, which resulted in higher levels of *Myb* transcription, all constructs induced comparable levels of *Myb* transcripts (data not shown). As we previously observed, pmel-1 $Myb^{\Delta/\Delta}$ Thy1.1⁺ T cells generated higher frequencies of T_{TE} cells at the peak of the immune response than did pmel-1 $Myb^{+/+}$ Thy1.1⁺T cells (Fig. 4b,c). As expected, fulllength c-Myb significantly reduced the percentage of T_{TE} cells (Fig. 4b,c). *Myb* (1–330) not only abolished the generation of T_{TE} cells but also dramatically increased the frequency of CD62L⁺ memory precursors (Fig. 4b,c), confirming the NRD's self-regulation of *Myb* in CD8⁺ T cells. Conversely, *Myb* pBind and *Myb* 304GP failed to rescue the phenotype of pmel-1 $Myb^{\Delta/\Delta}$ T cells (Fig. 4b,c), demonstrating the indispensable function of the c-Myb TAD in restraining CD8⁺ T cell terminal differentiation. Notably,

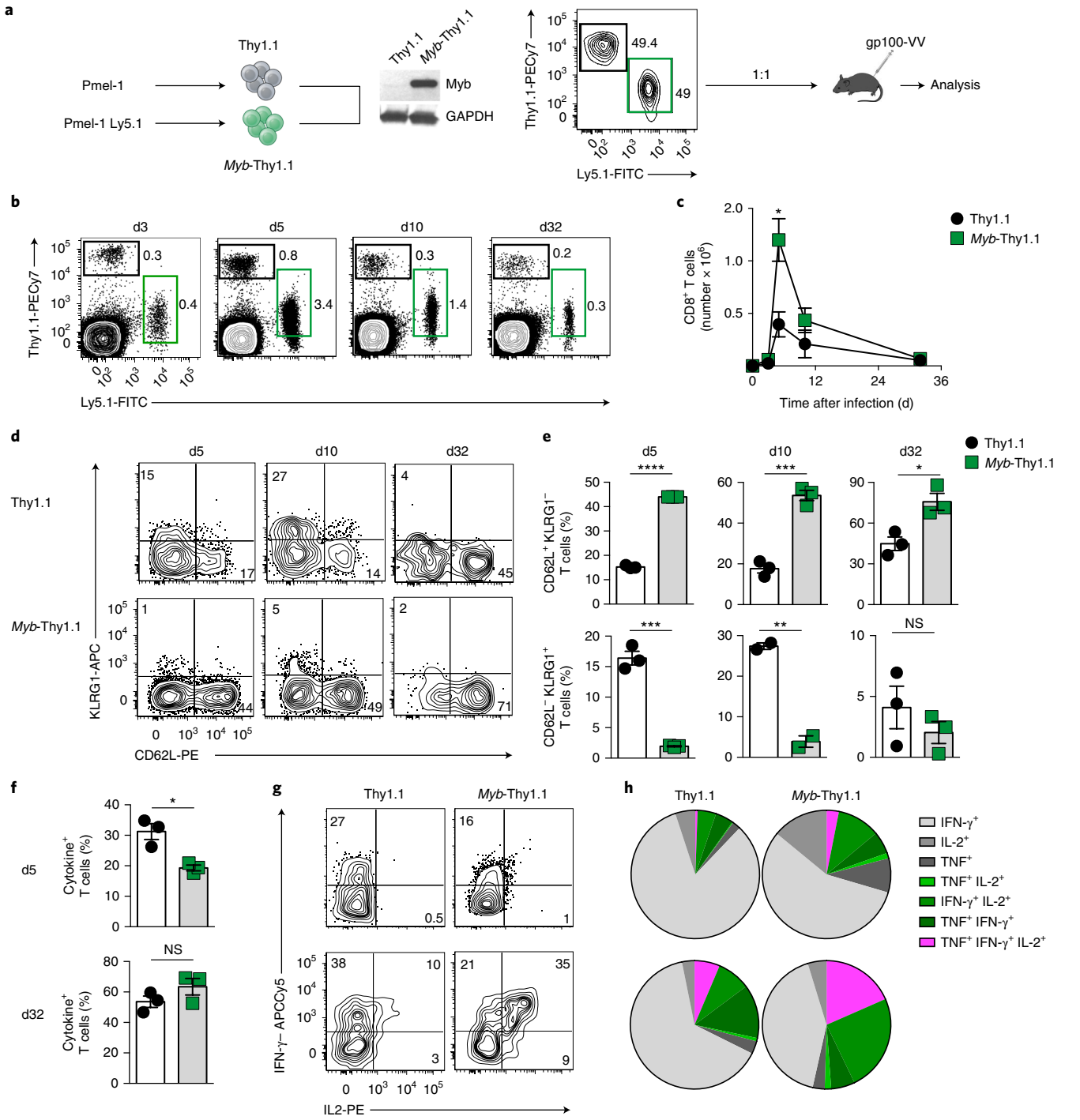

Fig. 5 | *Myb* overexpression enhances CD8⁺ T cell memory and polyfunctionality. a, Experimental design evaluating the impact of *Myb* overexpression in CD8⁺ T cell memory formation. Middle left, immunoblot of c-Myb in Thy1.1- and *Myb*-Thy1.1-overexpressing cells. Middle right, flow cytometry of the 1:1 mixture of Thy1.1⁺ and *Myb*-Thy1.1⁺ CD8⁺ T cells before transfer into mice (far right). **b**,**c**, Flow cytometry of splenic CD8⁺ T cells (**b**) and numbers of pmel-1 T cells (**c**) after co-transfer of 5×10^4 pmel-1-Thy1.1⁺ and 5×10^4 pmel-1 Ly5.1⁺ *Myb*-Thy1.1⁺ CD8⁺ T cells into wild-type mice infected with gp100-VV. Assessed 0–32 d after transfer ($n = 3$ mice per group per time point). **d**, Flow cytometry analysis of splenic pmel-1 T cells after transfer as in **b**,**c**. **e**, Percentage of KLRG1⁻CD62L⁺ (top row) and KLRG1⁺ CD62L⁻ (bottom row) splenic pmel-1 T cells after transfer as in **b**,**c**. **f**, Percentage of cytokine-producing pmel-1 T cells after transfer as in **b**,**c**. **g**,**h**, Intracellular cytokine staining (**g**) and combinatorial cytokine production (**h**) by splenic pmel-1 T cells 5 d after transfer as in **b**,**c**. Data are representative of two independent experiments. Data are shown after gating on live CD8⁺ cells (**b**) or live CD8⁺ Thy1.1⁺ cells (**d**,**g**). Data in **c**,**e**,**f** are shown as the mean ± s.e.m.; each symbol represents an individual mouse. $^*P < 0.05$, $^{**}P < 0.01$, $^{***}P < 0.001$ and $^{****}P < 0.0001$ (unpaired two-tailed Student's *t*-test).

these functional differences among the c-Myb mutants correlated with their abilities to induce *Tcf7* expression and repress *Zeb2* transcription. Full-length c-Myb and *Myb* (1–330), which both inhibited CD8⁺ T cell terminal differentiation, promoted *Tcf7* expression and decreased *Zeb2* transcripts compared with their expression in pmel-1 $Myb^{\Delta/\Delta}$ Thy1.1⁺ T cells (Fig. 4d,e). On the other hand,

Myb pBind, which did not rescue the phenotype of pmel-1 $Myb^{\Delta/\Delta}$ T cells, did not lower *Zeb2* expression and failed to induce *Tcf7* (Fig. 4d,e). *Myb* 304GP, which was inefficient in inhibiting CD8$^+$ T cell differentiation, did retain high levels of *Zeb2* and induce *Tcf7*, albeit to a lesser extent than did full-length c-Myb (Fig. 4d,e). This emphasizes the more prominent role of Zeb2 over that of Tcf1 in the regulation of T_{TE} cells. Thus, the c-Myb TAD restrains CD8$^+$ T cell differentiation by promoting *Tcf7* expression but mostly by suppressing *Zeb2* transcription. Despite being unable to correct CD8$^+$ T cell differentiation, *Myb* 304GP fully rescued the frequency and total number of pmel-1 $Myb^{\Delta/\Delta}$ T cells (Fig. 4f,g). Evidently, the pro-survival effects of c-Myb are independent of its TAD activity and its regulation of *Tcf7* and *Zeb2* (Fig. 3n,o). Further substantiating this conclusion is the finding that *Myb* (1–330), which markedly inhibited CD8$^+$ T cell differentiation, induced *Tcf7* and suppressed *Zeb2* expression but did not increase pmel-1 T cell frequency or total number to the levels produced by $Myb^{+/+}$ T cells (Fig. 4f,g). Combined with the results from *Myb* pBind complementation (Fig. 4f,g), the pro-survival activity of c-Myb is linked mainly to the integrity of its C-terminal domain. In summary, the c-Myb TAD is critical for regulating CD8$^+$ T cell differentiation, but it is the NRD that is essential for maintaining cell survival.

Enforced *Myb* expression enhances CD8$^+$ T cell stemness and polyfunctionality. Having demonstrated the pivotal role of c-Myb in the regulation of CD8$^+$ T cell stemness, we next sought to determine whether the generation of stem cell–like T_{CM} cells could be enhanced by enforcing *Myb* expression. We transduced pmel-1 Ly5.1$^+$ T cells with *Myb*-Thy1.1 and pmel-1 Ly5.2$^+$ T cells with Thy1.1 alone, mixed them at a 1:1 ratio and co-transferred them into wild-type mice infected with gp100-VV (Fig. 5a). Overexpression of c-Myb enhanced the expansion of splenic pmel-1 T cells, which accumulated at fourfold the rate of control cells at the peak of the immune response (Fig. 5b,c). Likewise, we observed increased expansion of *Myb*-overexpressing pmel-1 T cells in lungs and lymph nodes, although the accumulation was more pronounced in the latter (Supplementary Fig. 7a–d). Enforcing *Myb* expression did not increase the number of pmel-1 T cells in the spleen and lungs 30 d after transfer (Fig. 5b,c and Supplementary Fig. 7a,b), indicating that c-Myb overexpression alone is insufficient to cause unrestrained T cell expansion or transformation[20]. We observed, however, a dramatic increase in pmel-1 T cells (~50-fold) in the lymph nodes (Supplementary Fig. 7c,d), which prompted us to investigate whether the increased accumulation of *Myb*-overexpressing T cells in the lymph nodes was due to the preferential formation of stem cell–like T_{CM} cells, which preferentially home to lymphoid tissues. Consistent with our findings using c-Myb-deficient T cells, we found that overexpression of c-Myb promoted the generation of stem cell–like T_{CM} cells while restraining terminal effector differentiation (Fig. 5d,e and Supplementary Fig. 7e,f). These results were further strengthened by functional studies, which revealed that *Myb*-overexpressing cells displayed enhanced polyfunctionality and a sustained capacity to produce IL-2 (Fig. 5f–h). Taken together, these results demonstrate that increasing *Myb* levels in CD8$^+$ T cells is an effective strategy for generating polyfunctional stem cell–like T_{CM} cells.

Enforced expression of *Myb* enhances CD8$^+$ T cell recall responses and antitumor immunity. The hallmark of memory cells is their capacity to rapidly proliferate and differentiate into a massive number of effector cells after secondary infection. To determine whether enhanced generation of stem cell–like T_{CM} cells resulting from c-Myb overexpression would promote stronger recall responses, we re-challenged mice that were initially infected with gp100-VV with gp100-adV (Fig. 6a). Strikingly, the accumulation of splenic *Myb*-overexpressing T cells at the peak of the secondary immune response was 10-fold higher in frequency and number than that of control cells (Fig. 6b,c). Repeated antigen stimulations are known to drive CD8$^+$ T cells toward terminal differentiation[35,36]. To determine whether terminal differentiation could be restrained by overexpression of c-Myb, we measured T_{TE} cells after secondary infection with gp100-adV. Remarkably, c-Myb overexpression not only dramatically reduced the frequencies of T_{TE} cells in both peripheral and lymphoid tissues (Fig. 6d–i) but also maintained a higher fraction of stem cell–like T_{CM} cells. Moreover, intracellular cytokine staining analyses showed a marked reduction in terminally differentiated, monofunctional IFN-γ producers in the *Myb*-overexpression group (Fig. 6j–l).

It is well established that the dose of adoptively transferred tumor-specific CD8$^+$ T cells correlates with the magnitude of tumor regression[37]. Generating large numbers of tumor-reactive T cells in vitro can be counterproductive, however, because as cells expand they progressively differentiate into T_{TE} cells with limited therapeutic fitness[35]. We sought to determine whether overexpression of c-Myb would not only generate larger cell numbers through repetitive antigenic stimulations but also preserve a greater abundance of stem cell–like T_{CM} cells. As we previously showed, antigen re-stimulation induced the formation of CD62L$^-$ effector cells (Fig. 7a,b). By contrast, most pmel-1 T cells overexpressing c-Myb retained high CD62L expression throughout multiple stimulations (Fig. 7a,b). Notably, restimulated T cells preserved their mitochondrial mass only when c-Myb was constitutively overexpressed (Fig. 7c,d). Even after a multi-log expansion, *Myb*-overexpressing T cells exhibited significant SRC and fatty acid metabolism (Fig. 7e–g), highlighting the importance of c-Myb in the maintenance of metabolic fitness. To evaluate their therapeutic efficacy, we adoptively transferred multiply stimulated, *Myb*-overexpressing pmel-1 T cells into mice bearing subcutaneous B16-hgp100 melanomas in conjunction with the administration of IL-2. *Myb*-overexpressing T cells triggered curative responses in all mice, whereas controls cells failed to cure four out of five animals (Fig. 7h). Conversely, the antitumor efficacy of pmel-1 T cells was severely impaired in the absence of c-Myb (data not shown). To determine whether the transfer of stem cell–like T_{CM} cells in the *Myb*-overexpression group conferred long-lasting antitumor memory responses, we re-challenged the surviving animals with tumors around 200 d after the primary T cell transfer. Remarkably, tumors did not grow in any of the re-challenged animals (Fig. 7h), indicating that overexpression of c-Myb enhances the establishment of long-lived immunological memory. Consistent with this observation, we found increased numbers of memory T cells in the surviving mice that received *Myb*-overexpressing T cells 470 d earlier (Supplementary Fig. 8a,b). Although all memory T cells displayed a stem cell–like T_{CM} cell phenotype (Supplementary Fig. 8c), a larger fraction of *Myb*-overexpressing T cells than control cells was capable of producing IL-2 (Supplementary Fig. 8d). Taken together, these findings highlight the therapeutic potential of maneuvers aimed at increasing c-Myb activity in CD8$^+$ T cells.

Discussion

The molecular programs that regulate the formation and maintenance of stem cell–like T cells are not fully resolved. In this current study, we identified c-Myb as a master regulator of CD8$^+$ T cell stemness. In the absence of c-Myb, antigen-stimulated CD8$^+$ T cells are driven toward terminal effector differentiation and are prone to apoptosis, resulting in both qualitative and quantitative impairment of memory responses. These conclusions are further supported by the observation that CD8$^+$ T cells deficient in the microRNA miR-150, a known inhibitor of c-Myb, have an enhanced propensity to form long-lived memory T cells[38]. Our findings run parallel to those in stem cells and progenitor cells, in which c-Myb is seen to restrain differentiation[20,21], illuminating a conserved molecular program regulating self-renewal and differentiation[5].

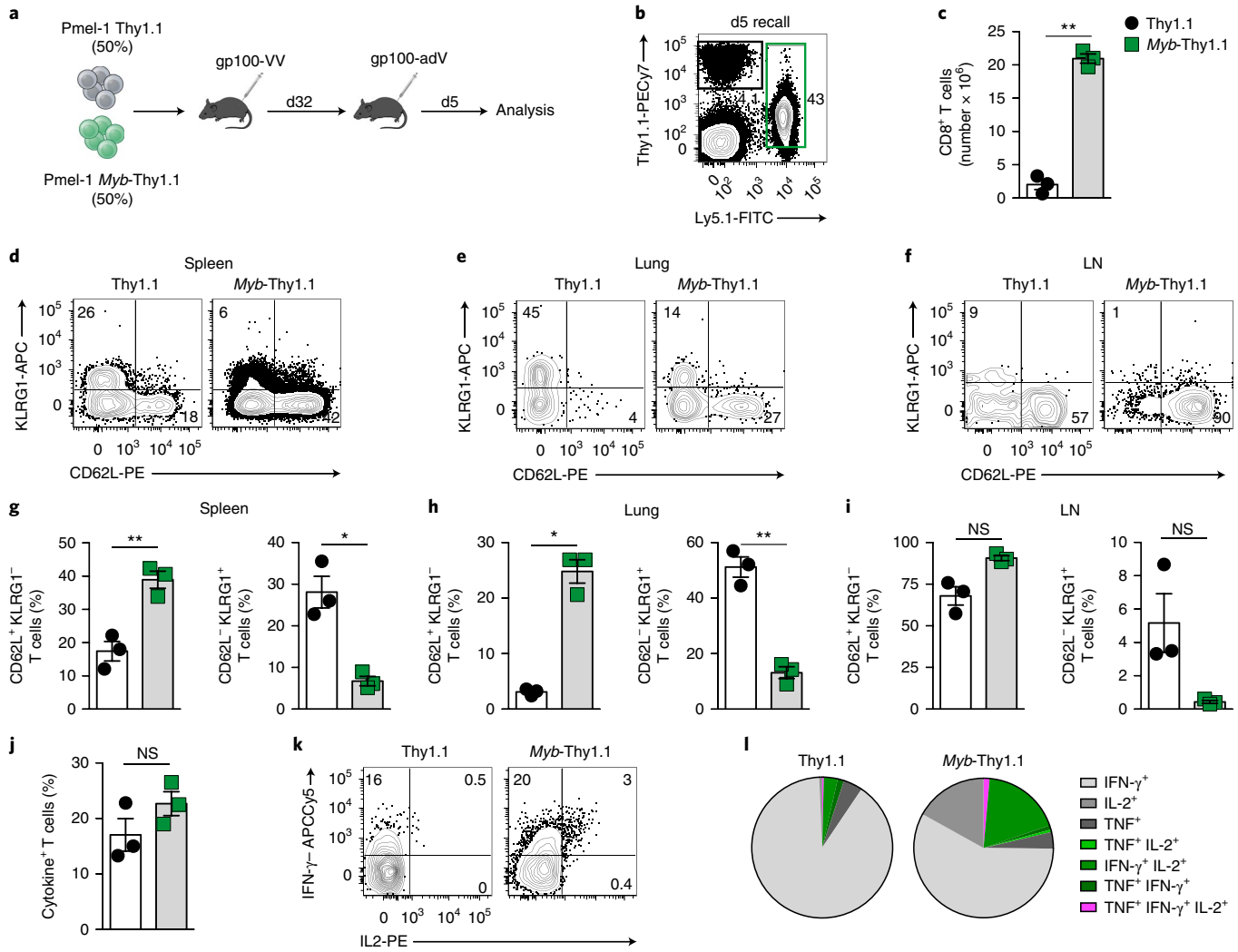

Fig. 6 | *Myb* overexpression enhances CD8⁺ T recall responses. a, Experimental design testing the impact of *Myb* overexpression on CD8⁺ T cell secondary responses. **b**,**c**, Flow cytometry of splenic CD8⁺ T cells (**b**) and numbers of pmel-1 CD8⁺ T cells (**c**) after co-transfer of 5×10^4 pmel-1-Thy1.1⁺ and 5×10^4 pmel-1 Ly5.1⁺ *Myb*-Thy1.1⁺ CD8⁺ T cells into wild-type mice infected with gp100-VV, assessed 5 d after secondary infection with gp100-adV ($n=3$ mice per group). **d**–**f**, Flow cytometry of pmel-1 T cells in the spleen (**d**), lungs (**e**) and lymph nodes (**f**) 5 d after secondary infection as in **b**,**c**. **g**–**i**, Percentage of KLRG1⁻CD62L⁺ and KLRG1⁺ CD62L⁻ pmel-1 T cells in the spleen (**g**), lungs (**h**) and lymph nodes (**i**) 5 d after secondary infection as in **b**,**c**. **j**, Percentage of cytokine⁺ splenic pmel-1 T cells 5 d after secondary infection as in **b**,**c**. **k**,**l**, Intracellular cytokine staining (**k**) and combinatorial cytokine production (**l**) by splenic pmel-1 T cells 5 d after secondary infection as in **b**,**c**. Data are representative of two independent experiments. Data are shown after gating on live CD8⁺ cells (**b**) or live CD8⁺ Thy1.1⁺ cells (**d**–**f**,**k**). Data in **c**,**g**–**j**, are shown as the mean ± s.e.m.; each symbol represents an individual mouse. $^*P<0.05$, $^{**}P<0.01$ (unpaired two-tailed Student's *t*-test).

Mechanistically, we demonstrated that c-Myb enhances CD8⁺ T cell survival and memory development by promoting expression of the gene encoding the anti-apoptotic molecule Bcl2 and by inducing *Tcf7*, which encodes a transcription factor (Tcf1) essential to the formation and maintenance of stem cell–like T_{CM} cells[13,14]. Recently, Tcf1 expression has also been associated with the maintenance of CXCR5⁺Tim3⁻ stem cell–like T cells in chronic infection and cancer[39–42]. Future work will determine whether c-Myb plays an important role in maintaining this cell population. We further demonstrated that c-Myb also actively repressed pro-differentiating programs by inhibiting the transcription of *Zeb2*, which encodes a transcription factor identified as a major driver of terminal effector differentiation[31]. This result further emphasizes the understudied repressive function of c-Myb, often considered a transcriptional activator. The repressive activity of c-Myb has been linked to its competitive binding with positive transcription regulators to target gene promoters[43] and to the recruitment of cell type–specific repressors[44,45]. While we have not formally addressed the latter mechanism, complementation studies with *Myb* pBind unequivocally excluded the possibility of a mechanism of competition with positive transcriptional regulators, as the c-Myb DNA-binding domain failed to suppress *Zeb2* transcription or restore physiological numbers of memory precursor cells on its own. Recently, it was proposed that c-Myb-mediated repression might paradoxically involve its interaction with the coactivator p300, possibly through the induction of repressive non-coding RNAs[28]. Consistent with this view, we found that *Myb* 304GP, which has been shown to have an impaired ability to recruit p300[34], was unable to repress *Zeb2* or inhibit terminal effector differentiation.

Our complementation studies also indicate that the C-terminal NRD domain of c-Myb has an important function in regulating CD8⁺ T cell survival. The mechanistic basis of this finding remains to be elucidated. Myb NRD contains an EVES motif that has been shown to bind p100[46]. Although p100 overexpression inhibited the

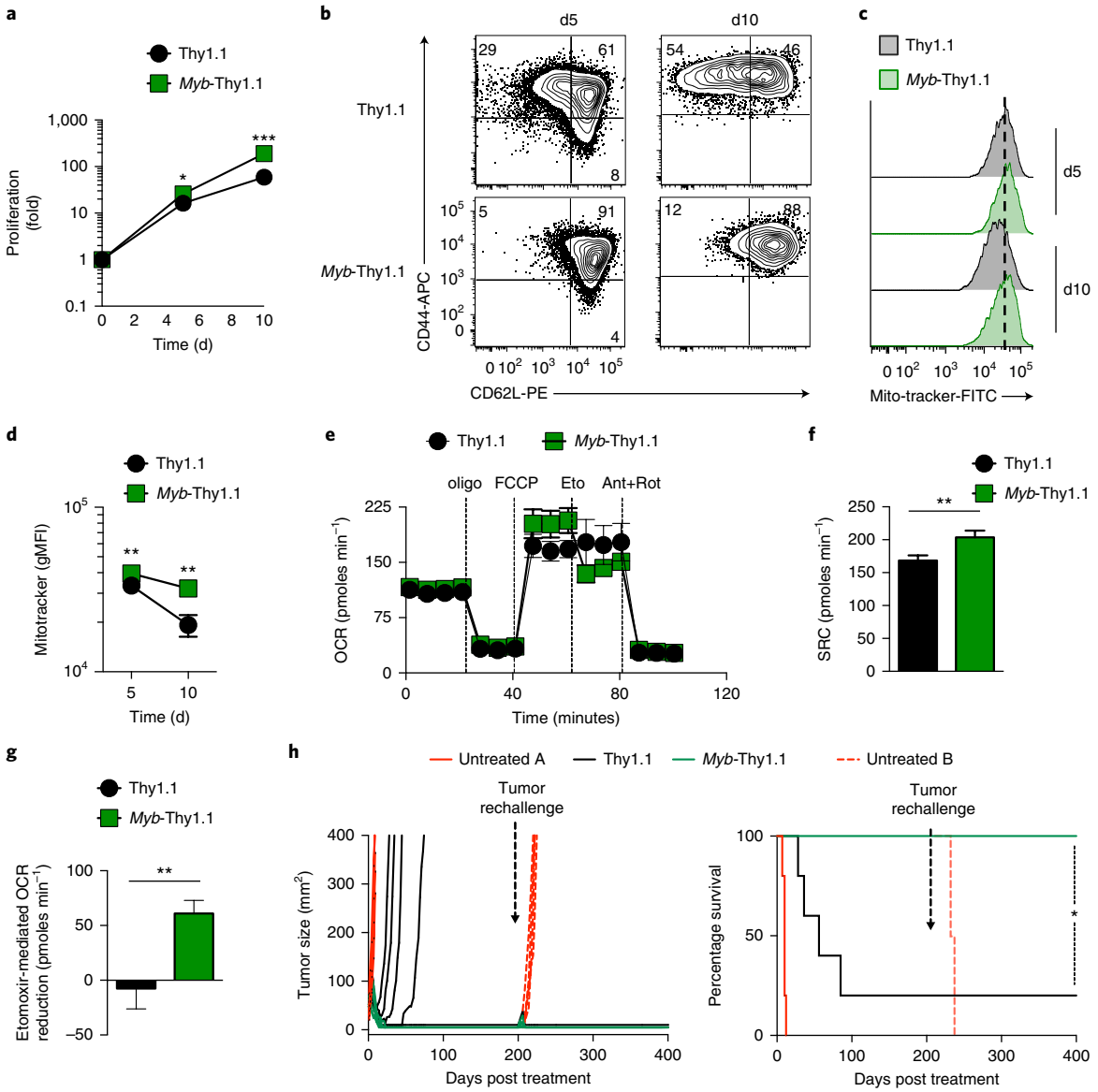

Fig. 7 | Enforced expression of *Myb* enhances CD8⁺ T cell antitumor immunity. a, Fold expansion of pmel-1 CD8⁺ T cells transduced with Thy1.1 or *Myb*-Thy1.1 after priming with antibodies to CD3 and CD28 and re-stimulation with the same antibodies 5 d later. Cells were grown in the presence of IL-2 throughout the culture ($n = 3$ independent experiments). **b**,**c**, Flow cytometry of pmel-1 T cells transduced with Thy1.1 or *Myb*-Thy1.1 generated as described in **a**. **d**, gMFI of Mitotracker staining in pmel-1 T cells generated as in **a**. ($n = 3$ technical replicates). **e**, OCR of pmel-1 T cells generated as in **a**, assessed at 10 d. Data were obtained under basal culture conditions and in response to the indicated molecules ($n = 12$ technical replicates). Eto, etomoxir. **e**–**g**, SRC (**e**,**f**) and reduction of OCR (**g**) after etomoxir administration in pmel-1 T cells generated as in **a**, assessed at 10 d ($n = 36$ technical replicates (12 replicates × three time points)). **h**, Tumor size (left) and survival (right) of wild-type mice bearing subcutaneous hgp100⁺ B16 melanoma cells after transfer of 5×10^6 pmel-1 T cells generated as in **a** in conjunction with gp100-VV and IL-2 ($n = 5$ mice per group). Solid and dashed red curve denotes tumor-challenged mice that received no T cell transfer. At 206 d after T cell transfer, mice were re-challenged with 2.5×10^5 hgp100⁺ B16 melanoma. Data are representative of two independent experiments. Tumor re-challenge after 200 d was performed in an individual experiment. Data are shown after gating on live CD8⁺ cells (**b**,**c**). Data in **a**,**d**–**g** are shown as the mean ± s.e.m.; each tumor curve represents an individual mouse. $^*P < 0.05$, $^{***}P < 0.001$ (**a**, unpaired two-tailed Student's *t*-test; **h**, log-rank (Mantel–Cox) test).

transcriptional activity of c-Myb in in vitro–cultured fibroblasts[46], this molecule has been demonstrated to function as a coactivator in other settings[47], possibly indicating its involvement in the pro-survival programs triggered by c-Myb.

Finally, our study has profound therapeutic implications for T cell–based immunotherapy. Uncoupling T cell differentiation from T cell expansion has been sought after as the 'holy grail' of adoptive immunotherapy, as the therapeutic efficacy depends considerably on both the cell dose and differentiation status of infused T cells[37,48]. Thus far, strategies that have been shown to effectively promote stem cell–like memory T cells have the downside effect of impairing cell expansion[4,17,49,50]. Overexpression of c-Myb not only preserved CD8⁺ T cell stemness by inhibiting differentiation but also allowed a better cell yield, resulting in curative antitumor responses and the establishment of long-term, tumor-specific immunologic memory. The *Myb* platform may ultimately pave new avenues for the generation of cell-based immunotherapy on the basis of the adoptive transfer of stem cell–like T_{CM} cells.

Online content

Any methods, additional references, Nature Research reporting summaries, source data, statements of data availability and associated accession codes are available at https://doi.org/10.1038/s41590-018-0311-z.

Received: 26 March 2018; Accepted: 19 December 2018;
Published online: 18 February 2019

References

1. Simons, B. D. & Clevers, H. Strategies for homeostatic stem cell self-renewal in adult tissues. *Cell* **145**, 851–862 (2011).
2. Graef, P. et al. Serial transfer of single-cell-derived immunocompetence reveals stemness of CD8$^+$ central memory T cells. *Immunity* **41**, 116–126 (2014).
3. Gattinoni, L. Memory T cells officially join the stem cell club. *Immunity* **41**, 7–9 (2014).
4. Gattinoni, L., Speiser, D. E., Lichterfeld, M. & Bonini, C. T memory stem cells in health and disease. *Nat. Med.* **23**, 18–27 (2017).
5. Gattinoni, L., Klebanoff, C. A. & Restifo, N. P. Paths to stemness: building the ultimate antitumour T cell. *Nat. Rev. Cancer* **12**, 671–684 (2012).
6. Thaventhiran, J. E., Fearon, D. T. & Gattinoni, L. Transcriptional regulation of effector and memory CD8$^+$ T cell fates. *Curr. Opin. Immunol.* **25**, 321–328 (2013).
7. Zhang, X. et al. FOXO1 is an essential regulator of pluripotency in human embryonic stem cells. *Nat. Cell Biol.* **13**, 1092–1099 (2011).
8. Yi, F. et al. Opposing effects of Tcf3 and Tcf1 control Wnt stimulation of embryonic stem cell self-renewal. *Nat. Cell Biol.* **13**, 762–770 (2011).
9. Niwa, H., Burdon, T., Chambers, I. & Smith, A. Self-renewal of pluripotent embryonic stem cells is mediated via activation of STAT3. *Genes Dev.* **12**, 2048–2060 (1998).
10. Ying, Q. L., Nichols, J., Chambers, I. & Smith, A. BMP induction of Id proteins suppresses differentiation and sustains embryonic stem cell self-renewal in collaboration with STAT3. *Cell* **115**, 281–292 (2003).
11. Hess Michelini, R., Doedens, A. L., Goldrath, A. W. & Hedrick, S. M. Differentiation of CD8 memory T cells depends on Foxo1. *J. Exp. Med.* **210**, 1189–1200 (2013).
12. Kim, M. V., Ouyang, W., Liao, W., Zhang, M. Q. & Li, M. O. The transcription factor Foxo1 controls central-memory CD8$^+$ T cell responses to infection. *Immunity* **39**, 286–297 (2013).
13. Jeannet, G. et al. Essential role of the Wnt pathway effector Tcf-1 for the establishment of functional CD8 T cell memory. *Proc. Natl Acad. Sci. USA* **107**, 9777–9782 (2010).
14. Zhou, X. et al. Differentiation and persistence of memory CD8$^+$ T cells depend on T cell factor 1. *Immunity* **33**, 229–240 (2010).
15. Cui, W., Liu, Y., Weinstein, J. S., Craft, J. & Kaech, S. M. An interleukin-21-interleukin-10-STAT3 pathway is critical for functional maturation of memory CD8$^+$ T cells. *Immunity* **35**, 792–805 (2011).
16. Ji, Y. et al. Repression of the DNA-binding inhibitor Id3 by Blimp-1 limits the formation of memory CD8$^+$ T cells. *Nat. Immunol.* **12**, 1230–1237 (2011).
17. Gattinoni, L. et al. A human memory T cell subset with stem cell-like properties. *Nat. Med.* **17**, 1290–1297 (2011).
18. Bender, T. P., Kremer, C. S., Kraus, M., Buch, T. & Rajewsky, K. Critical functions for c-Myb at three checkpoints during thymocyte development. *Nat. Immunol.* **5**, 721–729 (2004).
19. Dias, S. et al. Effector regulatory T cell differentiation and immune homeostasis depend on the transcription factor Myb. *Immunity* **46**, 78–91 (2017).
20. Ramsay, R. G. & Gonda, T. J. MYB function in normal and cancer cells. *Nat. Rev. Cancer* **8**, 523–534 (2008).
21. Greig, K. T., Carotta, S. & Nutt, S. L. Critical roles for c-Myb in hematopoietic progenitor cells. *Semin. Immunol.* **20**, 247–256 (2008).
22. Ji, Y. et al. Identification of the genomic insertion site of Pmel-1 TCR α and β transgenes by next-generation sequencing. *PLoS ONE* **9**, e96650 (2014).
23. Seibler, J. et al. Rapid generation of inducible mouse mutants. *Nucleic Acids Res.* **31**, e12 (2003).
24. Yuan, J., Crittenden, R. B. & Bender, T. P. c-Myb promotes the survival of CD4$^+$CD8$^+$ double-positive thymocytes through upregulation of Bcl-xL. *J. Immunol.* **184**, 2793–2804 (2010).
25. Jenkins, M. K. & Moon, J. J. The role of naive T cell precursor frequency and recruitment in dictating immune response magnitude. *J. Immunol.* **188**, 4135–4140 (2012).
26. Appay, V., van Lier, R. A., Sallusto, F. & Roederer, M. Phenotype and function of human T lymphocyte subsets: consensus and issues. *Cytometry. A.* **73**, 975–983 (2008).
27. van der Windt, G. J. et al. Mitochondrial respiratory capacity is a critical regulator of CD8$^+$ T cell memory development. *Immunity* **36**, 68–78 (2012).
28. Zhao, L. et al. Integrated genome-wide chromatin occupancy and expression analyses identify key myeloid pro-differentiation transcription factors repressed by Myb. *Nucleic Acids Res.* **39**, 4664–4679 (2011).
29. Taylor, D., Badiani, P. & Weston, K. A dominant interfering Myb mutant causes apoptosis in T cells. *Genes Dev.* **10**, 2732–2744 (1996).
30. Salomoni, P., Perrotti, D., Martinez, R., Franceschi, C. & Calabretta, B. Resistance to apoptosis in CTLL-2 cells constitutively expressing c-Myb is associated with induction of BCL-2 expression and Myb-dependent regulation of bcl-2 promoter activity. *Proc. Natl Acad. Sci. USA* **94**, 3296–3301 (1997).
31. Omilusik, K. D. et al. Transcriptional repressor ZEB2 promotes terminal differentiation of CD8$^+$ effector and memory T cell populations during infection. *J. Exp. Med.* **212**, 2027–2039 (2015).
32. Dominguez, C. X. et al. The transcription factors ZEB2 and T-bet cooperate to program cytotoxic T cell terminal differentiation in response to LCMV viral infection. *J. Exp. Med.* **212**, 2041–2056 (2015).
33. Boudousquie, C. et al. Differences in the transduction of canonical Wnt signals demarcate effector and memory CD8 T cells with distinct recall proliferation capacity. *J. Immunol.* **193**, 2784–2791 (2014).
34. Sandberg, M. L. et al. c-Myb and p300 regulate hematopoietic stem cell proliferation and differentiation. *Dev. Cell.* **8**, 153–166 (2005).
35. Gattinoni, L. et al. Acquisition of full effector function in vitro paradoxically impairs the in vivo antitumor efficacy of adoptively transferred CD8$^+$ T cells. *J. Clin. Invest.* **115**, 1616–1626 (2005).
36. Wirth, T. C. et al. Repetitive antigen stimulation induces stepwise transcriptome diversification but preserves a core signature of memory CD8$^+$ T cell differentiation. *Immunity* **33**, 128–140 (2010).
37. Klebanoff, C. A. et al. Determinants of successful CD8$^+$ T-cell adoptive immunotherapy for large established tumors in mice. *Clinical Cancer Res.* **17**, 5343–5352 (2011).
38. Chen, Z. et al. miR-150 regulates memory CD8 T cell differentiation via c-Myb. *Cell Reports* **20**, 2584–2597 (2017).
39. Im, S. J. et al. Defining CD8$^+$ T cells that provide the proliferative burst after PD-1 therapy. *Nature* **537**, 417–421 (2016).
40. Wu, T. et al. The TCF1-Bcl6 axis counteracts type I interferon to repress exhaustion and maintain T cell stemness. *Sci Immunol.* **1**, eaai8593 (2016).
41. Utzschneider, D. T. et al. T cell factor 1-expressing memory-like CD8$^+$ T cells sustain the immune response to chronic viral infections. *Immunity* **45**, 415–427 (2016).
42. Brummelman, J. et al. High-dimensional single cell analysis identifies stem-like cytotoxic CD8$^+$ T cells infiltrating human tumors. *J. Exp. Med.* **215**, 2520–2535 (2018).
43. Mizuguchi, G. et al. c-Myb repression of c-erbB-2 transcription by direct binding to the c-erbB-2 promoter. *J. Biol. Chem.* **270**, 9384–9389 (1995).
44. Reddy, M. A. et al. Opposing actions of c-ets/PU.1 and c-myb protooncogene products in regulating the macrophage-specific promoters of the human and mouse colony-stimulating factor-1 receptor (c-fms) genes. *J. Exp. Med.* **180**, 2309–2319 (1994).
45. Peng, S., Lalani, S., Leavenworth, J. W., Ho, I. C. & Pauza, M. E. c-Maf interacts with c-Myb to down-regulate Bcl-2 expression and increase apoptosis in peripheral CD4 cells. *Eur. J. Immunol.* **37**, 2868–2880 (2007).
46. Dash, A. B., Orrico, F. C. & Ness, S. A. The EVES motif mediates both intermolecular and intramolecular regulation of c-Myb. *Genes Dev.* **10**, 1858–1869 (1996).
47. Yang, J. et al. Identification of p100 as a coactivator for STAT6 that bridges STAT6 with RNA polymerase II. *EMBO J.* **21**, 4950–4958 (2002).
48. Crompton, J. G., Sukumar, M. & Restifo, N. P. Uncoupling T-cell expansion from effector differentiation in cell-based immunotherapy. *Immunol. Rev.* **257**, 264–276 (2014).
49. Gattinoni, L. et al. Wnt signaling arrests effector T cell differentiation and generates CD8$^+$ memory stem cells. *Nat. Med.* **15**, 808–813 (2009).
50. Sabatino, M. et al. Generation of clinical-grade CD19-specific CAR-modified CD8$^+$ memory stem cells for the treatment of human B-cell malignancies. *Blood* **128**, 519–528 (2016).
57. Roychoudhuri, R. et al. Transcriptional profiles reveal a stepwise developmental program of memory CD8$^+$ T cell differentiation. *Vaccine* **33**, 914–923 (2015).

Acknowledgements

This work was supported by the Intramural Research Program of the US National Institutes of Health, National Cancer Institute, Center for Cancer Research (ZIABC011480) (to L.G.); the US National Institutes of Health grants (GM100776 and CA85842) (to T.P.B.); the Wellcome Trust/Royal Society (105663/Z/14/Z), the UK Biotechnology and Biological Sciences Research Council (BB/N007794/1) and Cancer Research UK (C52623/A22597) (to R.R.). We thank K. Hanada for providing B16 (H-2^b)-hgp100. This work used the computational resources of the NIH HPC Biowulf cluster (http://hpc.nih.gov).

Author contributions

S.G., J.F., J.B.L, P.B., N.E.L., J.H., J.D.H., N.V.H., V.K., W.G.T., D.G., R.R. and Y.J. performed the experiments. S.G., W.Z., J.B.L., Y.J. and L.G. analyzed the experiments. S.G., B.W.H., R.R., N.P.R., T.P.B. and L.G. designed the experiments. Z.Y., H.H.X., A.B. and T.P.B. contributed reagents. W.Z., J.B.L., R.R., N.P.R., T.P.B. and Y.J. edited the manuscript. S.G. and L.G wrote the manuscript.

Competing interests

P.B. and B.W.H. are full-time employees of MedImmune and have stock in AstraZeneca. S.G., Y.J. and L.G. have a pending patent on c-Myb technology.

Additional information

Supplementary information is available for this paper at https://doi.org/10.1038/s41590-018-0311-z.

Reprints and permissions information is available at www.nature.com/reprints.

Correspondence and requests for materials should be addressed to L.G.

Publisher's note: Springer Nature remains neutral with regard to jurisdictional claims in published maps and institutional affiliations.

Methods

Mice. C57BL/6NCr and B6-Ly5.1/Cr were from Charles River Frederick Research Model Facility; pmel-1 (B6. Cg-*Thy1*^{a}/Cy Tg(TcraTcrb)8Rest/J) mice were from the Jackson Laboratory; Cre-ER^{T2} (B6-*Gt(ROSA)26Sor*$^{tm9(cre/Esr1)Arte}$) mice were from Taconic. *Myb*$^{fl/fl}$ mice[18] were obtained from T. Bender, University of Virginia, Charlottesville and were back-crossed with C57BL/6NCr mice for >30 generations; *Zeb2*$^{fl/fl}$ mice were kindly obtained from S. Kaech, Yale University, New Heaven. Pmel-1 mice were crossed with *Myb*$^{fl/fl}$ mice for the generation of pmel-1 *Myb*$^{fl/fl}$ mice and were further crossed with *Cre-ER*^{T2} mice for the generation of pmel-1 *Cre-ER*^{T2} *Myb*$^{fl/fl}$ mice. pmel-1 Cre-ER^{T2} *Myb*$^{fl/fl}$ mice were further crossed with *Zeb2*$^{fl/fl}$ mice to obtain pmel-1 *Cre-ER*^{T2} *Myb*$^{fl/fl}$ *Zeb2*$^{wt/fl}$ mice. Spleens from *Tcf7*$^{GFP/+}$ mice[51] were obtained from A. Bhandoola, National Cancer Institute and H.-H. Xue, Iowa University. All mouse experiments were done with the approval of the National Cancer Institute Animal Care and Use Committee.

Cell lines. Platinum-E cells were obtained from Cell Biolabs following authentication and validation as being mycoplasma free. B16 melanoma expressing human gp100 (B16-hgp100)[52] were provided by K.-I. Hanada, National Cancer Institute, Bethesda, and validated as being mycoplasma free via a PCR-based assay.

Antibodies, flow cytometry and cell sorting. Antibody to BrdU (anti-BrdU) (3D4), anti-Ly5.2 (104), anti-Thy1.1 (OX-7), anti-CD62L (MEL-14), anti-IFNγ (XMG1.2), anti-TNF (MP6-XT2) were from BD Biosciences; anti-CD8α (53-6.7), anti-KLRG-1 (2F1), anti-IL-2 (JE56-5H4), anti-CD44 (IM7), Bcl-2 (633504), anti–mouse perforin (S16009A) and anti–human/mouse granzyme B (GB11) were from Biolegend; anti-TCF1 (C63D9) was from Cell Signaling Technology. For intracellular staining of Tcf1, Bcl-2, granzyme B and perforin, cells were fixed and permeabilized (eBioscience, 00-5524). Leukocyte Activation Cocktail containing phorbol myristate acetate and ionomycin (BD Biosciences) was used to stimulate T cells for intracellular cytokine staining. A Fixation/Permeabilization Solution Kit (BD Biosciences) was used to fix and permeabilize the cells. Annexin V staining was performed with an Annexin V Apoptosis Detection Kit (eBiosciences). BrdU staining was performed with a BrdU Staining Kit (eBiosciences) following the protocol provided by the manufacturer. LSR II or BDFortessa (BD Biosciences) were used for flow cytometry acquisition. Samples were analyzed with FlowJo software (TreeStar). Naive CD8^{+} T cells were enriched using a Naïve CD8^{+} T cell isolation kit from Stem Cell Technology. A FACSAria (BD Biosciences) was employed for all other T cell enrichments.

Real-time RT–PCR. RNA was isolated with an RNeasy Mini Kit (Qiagen). RT–PCR was performed to obtain complimentary DNA (Applied Biosystems). Primers from Applied Biosystems and a Prism 7900HT (Applied Biosystems) were used for real-time PCR using Fast Start Universal SYBR GREEN Master (Roche). Results are presented relative to *Actb* or *Rpl13* expression.

List of primers used:
*Rpl13*F: CGAGGCATGCTGCCCCACAA
*Rpl13*R: AGCAGGGACCACCATCCGCT
*Bcl2*F: GTCGCTACCGTCGTGACTTC
*Bcl2*R: CAGACATGCACCTACCCAGC
*Zeb2*F: CCACGCAGTGAGCATCGAA
*Zeb2*R: CAGGTGGCAGGTCATTTTCTT
*Myb*F: AGACCCCGACACAGCATCTA
*Myb*R: CAGCAGCCCATCGTAGTCAT
*Tcf7*F: AGCTTTCTCCACTCTACGAACA
*Tcf7*R: AATCCAGAGAGATCGGGGGTC
*Eomes*F: GCGCATGTTTCCTTTCTTGAG
*Eomes*R: GGTCGGCCAGAACCACTTC
*Tbx21*F: AGCAAGGACGGCGAATGTT
*Tbx21*R: GGGTGGACATATAAGCGGTTC
*Prdm1*F: TTCTCTTGGAAAAACGTGTGGG
*Prdm1*R: GGAGCCGGAGCTAGACTTG
*Bach2*F: TCAATGACCAACGGAAGAAGG
*Bach2*R: GTGCTTGCCAGAAGTATTCACT

Immunoblot analysis. Proteins were separated by 4–12% SDS-PAGE, followed by standard immunoblot analysis with anti-Myb (Millipore, clone 1-1), anti-GAPDH (6C5; Santa Cruz Biotechnology), horseradish peroxidase–conjugated goat anti–mouse IgG (sc-2031; Santa Cruz Biotechnology) and horseradish peroxidase–conjugated goat anti–rabbit IgG (sc-2030; Santa Cruz Biotechnology).

Chromatin immunoprecipitation. 5-day in vitro–cultured cells were crosslinked to chromatin by adding 1% formaldehyde to each culture dish at room temperature for 10 min, and this was stopped by the addition of 125 mM glycine, followed by incubation at room temperature for 5 min. Cells were harvested, pelleted and washed with cold PBS. Cells were resuspended at 10^{7} cells per ml in cold cytoplasmic lysis buffer (20 mM Tris-HCl, pH 8, 85 mM KCl, 0.5% NP-40, 1 mM phenylmethyl sulfonyl fluoride (PMSF) and EDTA-free protease inhibitor mixture (Roche)) and were incubated on ice for 10 min. Nuclei were centrifuged, resuspended at 10^{7} cells per ml in cold sonication buffer (10 mM Tris-HCl, pH 8, 0.1 mM EDTA, 1% NP-40, 0.01% SDS, 1 mM PMSF and EDTA-free protease inhibitor mixture) and sonicated using a Branson 450 sonifier to generate chromatin fragment. Debris were cleared by centrifugation, and chromatin was supplemented with 5% glycerol and 127 mM NaCl. Chromatin aliquots of 500 µl were pre-cleared using protein A agarose slurry (Millipore) for 1 h and were immunoprecipitated overnight with anti-Myb (A304-138A; Bethyl) or mouse IgG2a,κ isotype-matched control antibody (BD Biosciences) with rotation at 4 °C. Immunocomplexes were collected with protein A agarose slurry for 1 h with rotation at 4 °C. Beads were washed for 5 min with rotation at 4 °C with low salt buffer (10 mM Tris-HCl, pH 8, 2 mM EDTA, 0.1% SDS, 1% NP40, 150 mM NaCl), high-salt buffer (10 mM Tris-HCl, pH8, 2 mM EDTA, 0.1% SDS, 1% NP40 and 500 mM NaCl), LiCl buffer (10 mM Tris-HCl, pH 8, 1 mM EDTA, 1% deoxycholate, 1% NP40 and 250 mM LiCl) and twice in TE. All wash buffers were supplemented with protease inhibitors and PMSF. Bound complexes were eluted off the beads in 500 µl elution (0.1 M, 1% SDS) buffer with rotation at room temperature for 30 min. Formaldehyde crosslinking was reversed in the presence of 200 mM NaCl at 65 °C overnight. DNA was phenol/chloroform extracted following RNAse A and proteinase K treatment.

ChIP-PCR primers. *Tcf7*F 5′- ATAACTGGTGCCATGACCGG-3′
Tcf7R 5′- CAGGGCTGGACAACACAAAG -3′
Zeb2 primers were from Qiagen (GPM1048638(+)04 A).

Retroviral vector construction and virus production. *Myb* isoform 2 or its mutants' cDNA was cloned together into the MSGV-1-Thy1.1 vector as previously described[16]. Platinum-E cell lines were used for gamma-retroviral production by transfection with DNA plasmids through the use of Lipofectamine 2000 (Invitrogen) and collection of virus 40 h after transfection. pMIG empty vector and *Tcf7*- pMIG were obtained from A. Bhandoola, National Cancer Institute.

In vitro activation and transduction of CD8^{+} T cells. Naïve CD8^{+} T cells were activated on plates coated with anti-CD3ε (2 µg ml^{-1}; 145-2C11; BD Biosciences) and soluble anti-CD28 (1 µg ml^{-1}; 37.51; BD Biosciences) in culture medium containing recombinant human IL-2 (10 ng ml^{-1}; Prometheus Laboratories). Virus was 'spin-inoculated' at 2,000*g* for 2 h at 32 °C onto plates coated with retronectin (Takara). CD8^{+} T cells activated for 24 h were spun onto plates after aspiration of viral supernatants. Transduction efficiency was then evaluated 48 h later.

Tamoxifen treatment, adoptive cell transfer, infection and tumor challenge. Cre-ERT2-mediated deletion of *lox*P-flanked alleles was induced by intraperitoneal injection of 2 mg tamoxifen (Sigma-Aldrich) dissolved in corn oil (Sigma-Aldrich) for 4 consecutive days. Pmel-1 CD8^{+} T cells (600×10^{5} to 3×10^{5} cells) were adoptively transferred into 6- to 10-week-old C57BL/6, followed by infection with 2×10^{7} PFU recombinant vaccinia virus expressing human gp100 (gp100-VV). Recall response experiments were performed 30–45 d after primary infection with gp100-VV by either re-challenge of mice with 10^{8} PFU recombinant adenovirus type 2 expressing human gp100 or secondary adoptive transfer of normalized memory cell numbers. For homeostatic proliferation of memory CD8^{+} T cells, recipient mice were sub-lethally irradiated (5 Gy) before cell transfer. For tumor experiments 6- to 10-week-old C57BL/6 mice were injected subcutaneously with 2×10^{5} B16-hgp100. Mice were treated 10 d later by intravenous injection of 5×10^{6} pmel-1 CD8^{+} T cells. Mice were vaccinated intravenously with 2×10^{7} PFU gp100-VV and recombinant human IL-2 (2.4e5 IU per dose) was administered twice a day for a total of six doses. For long-term memory and secondary transfer experiments, we employed recipient mice carrying the *Myb*^{fl} allele to avoid possible rejection. In these experiments, we used pmel CD8^{+} T cells from tamoxifen-treated littermates carrying the *Myb*^{fl} allele but not cre*ER*^{T2} as wild-type controls.

Quantification of adoptively transferred cells. Spleens were processed and cells were counted by trypan blue exclusion of dead cells. The frequency of transferred T cells was determined by measurement of the expression of CD8 and Thy1.1 or GFP or Thy1.1/Ly5.1 or Ly5.2 by flow cytometry. The absolute number of pmel-1 cells was calculated by multiplying the total cell count by the percentage of CD8^{+}GFP^{+}, CD8^{+}Thy1.1^{+} or CD8^{+}Thy1.1^{+} Ly5.1^{+} cells or CD8^{+}Ly5.2^{+} cells.

Bioenergetics analyses. CD8^{+} T cells were resuspended in serum-free unbuffered DMEM medium (Sigma-Aldrich) supplemented with L-glutamine (200 mM), NaCl (143 mM), D-glucose (25 mM) and sodium pyruvate (1 mM). Cells were then plated onto Seahorse cell plates (10^{6} cells per well) coated with Cell-Tak (Corning) to facilitate T cell attachment. Mitochondrial stress test was performed by measuring OCR (pmol min^{-1}) at steady state and after sequential injection of oligomycin (0.5 µM), FCCP (0.5 µM), rotenone (1 µM) and antimycin A (1 µM) (Sigma-Aldrich). In some experiments, etomoxir (43 µM) was injected before rotenone and antimycin A. Experiments with the Seahorse system used the following assay conditions: 2 min mixture; 2 min wait; and 3 min measurement.

RNA-seq. RNA concentration was determined with the Qubit RNA broad range assay in the Qubit Fluorometer (Invitrogen), and RNA integrity was determined with Eukaryote Total RNA Nano Series II Chip on a 2100 Bioanalyzer (Agilent).

RNA-seq libraries were prepared from 4 µg of total RNA via the TruSeq RNA sample prep kit according to manufacturer's protocol (Illumina). In brief, oligo(dT)-purified mRNA was fragmented and subjected to first- and second-strand cDNA synthesis. cDNA fragments were blunt-ended, ligated to Illumina adapters and PCR amplified to enrich for the fragments ligated to adapters. The resulting cDNA libraries were verified and quantified on Agilent Bioanalyzer, and sequencing (2 × 75 base pair paired-end) was conducted on a GAIIx Genome Analyzer (Illumina). RNA-seq analyses were performed using three biological replicates. RNA sequencing was performed and analyzed as described previously. Briefly, total RNA was prepared from cells using the RNeasy Plus Mini Kit (Qiagen). 200 ng total RNA was subsequently used to prepare the RNA-seq library by using TruSeq RNA sample prep kit (FC-122-1001, Illumina) according to the manufacturer's instructions. Sequenced reads were aligned to the mouse genome (NCBI37/mm9) with TopHat v.2.0.11[53], and uniquely mapped reads were used to calculate gene expression. The mouse genome reference sequences (mm9) and the genome annotation were downloaded from the UCSC genome browser for RNA-seq analysis. Raw counts that fell on transcripts of each gene were calculated, and differentially expressed genes were identified with the statistical R package DESeq2[54]. Differentially expressed genes were required to meet to the criteria: fold change >1.5 or <1.5, and false discovery rate <0.05. Expression heatmaps were generated with the Bioconductor Package ComplexHeatmap[55].

Gene-set enrichment and pathway analyses. Mouse gene symbols were first mapped to the orthologous human genes using the homology information available from the MGI website (ftp://ftp.informatics.jax.org/pub/reports/HMD_HGNC_Accession.rpt) and were ranked by the fold changes of the gene expression as profiled by RNA-seq. Then, gene-set enrichment was analyzed using GSEA software (http://software.broadinstitute.org/gsea/downloads.jsp)[56]. Pathway analysis was performed on the identified differentially expressed genes list using the Core Analysis function included in Ingenuity Pathway Analysis (IPA, Qiagen).

CFSE and MitoTracker Green labeling. $CD8^+$ T cells were incubated with 1 µl of CFSE (Thermo Fischer no. C34554) in 1 ml protein-free PBS for 20 min at 37 °C with agitation followed. For MitoTracker Green staining, $CD8^+$ T cells were incubated with 250 nM MitoTracker Green FM (Molecular Probes) for 30 min at 37 °C.

Cytolytic assay. Target-cell lysis was evaluated with the xCELLigence Real-Time Cell Analyzer (ACEA Biosciences). Electrical impedance due to B16-hgp100 was measured every 15 min until the end of the experiment. The data were processed using the xCELLigence RTCA software package (v.2.0), and the results are reported as a cell index value (CI), where CI = (impedance at time point *n* – impedance in the absence of cells) / nominal impedance value. Cell index was normalized to 1 at the time when T cells were added. Percentage of lysis was calculated for values obtained after 18 h of co-culture and different T cell/B16-hgp100 ratios.

Statistical analyses. Using Graphpad Prism 7, a two-tailed Student's *t*-test was used for comparison of data such as gene expression levels, cell proliferation and functionality (numbers and percentage) and tumor growth slopes. A log-rank (Mantel–Cox) test was used for comparison of survival curves.

Reporting Summary. Further information on research design is available in the Nature Research Reporting Summary linked to this article.

Data availability

RNA-seq data are deposited to the Gene Expression Omnibus (GEO) under accession number GSE112049. All other data that support the findings of this study are available from the corresponding author upon request.

References

51. Yang, Q. et al. TCF-1 upregulation identifies early innate lymphoid progenitors in the bone marrow. *Nat. Immunol.* **16**, 1044–1050 (2015).
52. Eil, R. et al. Ionic immune suppression within the tumour microenvironment limits T cell effector function. *Nature* **537**, 539–543 (2016).
53. Kim, D. et al. TopHat2: accurate alignment of transcriptomes in the presence of insertions, deletions and gene fusions. *Genome. Biol.* **14**, R36 (2013).
54. Love, M. I., Huber, W. & Anders, S. Moderated estimation of fold change and dispersion for RNA-seq data with DESeq2. *Genome. Biol.* **15**, 550 (2014).
55. Gu, Z., Eils, R. & Schlesner, M. Complex heatmaps reveal patterns and correlations in multidimensional genomic data. *Bioinformatics* **32**, 2847–2849 (2016).
56. Subramanian, A. et al. Gene set enrichment analysis: a knowledge-based approach for interpreting genome-wide expression profiles. *Proc. Natl Acad. Sci. USA* **102**, 15545–15550 (2005).

nature research

Corresponding author(s): Luca Gattinoni

Last updated by author(s): 2018/12/17

Reporting Summary

Nature Research wishes to improve the reproducibility of the work that we publish. This form provides structure for consistency and transparency in reporting. For further information on Nature Research policies, see Authors & Referees and the Editorial Policy Checklist.

Statistics

For all statistical analyses, confirm that the following items are present in the figure legend, table legend, main text, or Methods section.

n/a	Confirmed	
☐	☒	The exact sample size (*n*) for each experimental group/condition, given as a discrete number and unit of measurement
☐	☒	A statement on whether measurements were taken from distinct samples or whether the same sample was measured repeatedly
☐	☒	The statistical test(s) used AND whether they are one- or two-sided *Only common tests should be described solely by name; describe more complex techniques in the Methods section.*
☒	☐	A description of all covariates tested
☒	☐	A description of any assumptions or corrections, such as tests of normality and adjustment for multiple comparisons
☐	☒	A full description of the statistical parameters including central tendency (e.g. means) or other basic estimates (e.g. regression coefficient) AND variation (e.g. standard deviation) or associated estimates of uncertainty (e.g. confidence intervals)
☒	☐	For null hypothesis testing, the test statistic (e.g. *F*, *t*, *r*) with confidence intervals, effect sizes, degrees of freedom and *P* value noted *Give P values as exact values whenever suitable.*
☒	☐	For Bayesian analysis, information on the choice of priors and Markov chain Monte Carlo settings
☒	☐	For hierarchical and complex designs, identification of the appropriate level for tests and full reporting of outcomes
☒	☐	Estimates of effect sizes (e.g. Cohen's *d*, Pearson's *r*), indicating how they were calculated

Our web collection on statistics for biologists contains articles on many of the points above.

Software and code

Policy information about availability of computer code

Data collection	BD FACSDivaTM 8.0, BioRADXF Manager 3.0, Wave-Seahorse 2.4.1, Illumina Casava suite v1.8.2
Data analysis	Flowjo_v9.9.4, GraphPad Prism 7, Microsoft Excel, R package ggplot2,TopHat 2.0.1151, DSEq2, GSEA, Ingenuity Pathway Analysis 2.4.10, xCELLingence RTCA 2.0.

For manuscripts utilizing custom algorithms or software that are central to the research but not yet described in published literature, software must be made available to editors/reviewers. We strongly encourage code deposition in a community repository (e.g. GitHub). See the Nature Research guidelines for submitting code & software for further information.

Data

Policy information about availability of data

All manuscripts must include a data availability statement. This statement should provide the following information, where applicable:

- Accession codes, unique identifiers, or web links for publicly available datasets
- A list of figures that have associated raw data
- A description of any restrictions on data availability

RNA-seq data are deposited to the Gene Expression Omnibus (GEO) under accession number GSE112049. All other data that support the findings of this study are available from the corresponding author upon request.

Field-specific reporting

Please select the one below that is the best fit for your research. If you are not sure, read the appropriate sections before making your selection.

☒ Life sciences ☐ Behavioural & social sciences ☐ Ecological, evolutionary & environmental sciences

For a reference copy of the document with all sections, see nature.com/documents/nr-reporting-summary-flat.pdf

Life sciences study design

All studies must disclose on these points even when the disclosure is negative.

Sample size	For tumor experiments we employed 5 animal/group. For T cell kinetic and functional studies we employed 3 animals/group per each time point. These sample sizes allow for statistically valid comparisons based on previous studies conducted by this laboratory. RNA-seq were done in triplicate samples of two animals for each group (KLRG1negCD62Lneg WT versus KLRG1negCD62Lneg MybKO). The sample size was based on previous studies conducted by this laboratory which allow for statistically valid comparisons.
Data exclusions	No data from the study were excluded.
Replication	All data were reliably reproduced in at least two independent experiments with the exception of the RNA-seq analysis which was performed once on triplicate samples obtained from two pooled mice for each group. Key RNA-seq findings were independently validated with qPCR. The tumor re-challenge experiment performed at 204 days post-transfer and the tumor experiment testing MybKO T cells were performed once. The experiments evaluating in vivo CD8 T cell stemness were also performed once.
Randomization	For all animal experiments, mice were randomly assigned to different treatment and control groups.
Blinding	Tumor size were blindly measured. All other data were acquired and analyzed in a non-blind fashion because did not involve subjective measurements.

Reporting for specific materials, systems and methods

We require information from authors about some types of materials, experimental systems and methods used in many studies. Here, indicate whether each material, system or method listed is relevant to your study. If you are not sure if a list item applies to your research, read the appropriate section before selecting a response.

Materials & experimental systems

n/a	Involved in the study
☐	☒ Antibodies
☐	☒ Eukaryotic cell lines
☒	☐ Palaeontology
☐	☒ Animals and other organisms
☒	☐ Human research participants
☒	☐ Clinical data

Methods

n/a	Involved in the study
☒	☐ ChIP-seq
☐	☒ Flow cytometry
☒	☐ MRI-based neuroimaging

Antibodies

Antibodies used

BD Biosciences: anti-BrdU (clone 3D4) catalog# 51-23614L, anti-Ly5.2 (clone 104) catalog# 553772, anti-Thy1.1 (clone OX-7) catalog# 25-0900-82, anti-CD62L (clone MEL-14) catalog# 553151, anti-IFN (clone XMG1.2) catalog# 557998, anti-TNF (clone MP6-XT2) catalog# 17-7321-82.

Biolegend: anti-CD8α (clone 53-6.7) catalog# 100714, anti-KLRG-1 (clone 2F1) catalog# 138412, anti-IL-2 (clone JE56-5H4) catalog# 503808, anti-CD44 (clone IM7) catalog# 103043, Bcl-2 (clone 633504) catalog# 633504, anti-mouse Perforin Antibody (clone S16009A) catalog# 154406, anti-human/mouse granzyme B Antibody (clone GB11) catalog# 515408

Cell Signaling Technology: anti-TCF1 (clone C63D9) catalog#655204

Millipore: anti-c-Myb (clone 1-1) catalog# 05-175 dilution: 1/1,000

Santa Cruz Biotechnology: anti-GAPDH (clone 6C5) catalog # sc-32233 dilution: 1/2,000
horseradish peroxidase–conjugated goat anti–mouse IgG (polyclonal) catalog # sc-2031 dilution: 1/50,000; horseradish peroxidase–conjugated goat anti–rabbit IgG (polyclonal) catalog # sc-2030 dilution: 1/50,000.

All FACS antibodies were titered to determine the maximum dilution to achieve population separation without observable background.

Validation	All antibodies are commercially available and validated by previous studies performed in other and our laboratory.

Eukaryotic cell lines

Policy information about cell lines

Cell line source(s)	B16 (H-2b)-hgp100 was obtained from Hanada K. (NCI), NIH. Platinum-E cell lines were obtained from Cell Biolabs.
Authentication	B16-hgp100 cells were validated by morphology, pigmentation and recognition by gp100-specific TCR transgenic CD8+ T cells. Platinum Eco cell lines were validated by the vendor, and by the authors' assessment of cell morphology and ability to produce retro-viral particles.
Mycoplasma contamination	Platinum-E cells and B16-hgp100 were validated as being mycoplasma free via a PCR-based assay.
Commonly misidentified lines (See ICLAC register)	No commonly misidentified lines were used

Animals and other organisms

Policy information about studies involving animals; ARRIVE guidelines recommended for reporting animal research

Laboratory animals	C57BL/6NCr and B6-Ly5.1/Cr were from Charles River Frederick Research Model Facility; pmel-1 (B6. Cg-Thy1a/Cy Tg(TcraTcrb)8Rest/J) mice were from the Jackson Laboratory; Cre-ERT2 (B6-Gt(ROSA)26Sortm9(cre/Esr1)Arte) mice were from Taconic. Mybfl/fl mice18 were obtained from Timothy Bender, University of Virginia, Charlottesville, VA and were back-crossed with C57BL/6NCr mice for >30 generations, USA; Zeb2fl/fl mice were kindly obtained from Susan Kaech, Yale University, New Heaven, CT, USA. Pmel-1 mice were crossed with Mybfl/fl mice for the generation of pmel-1 Mybfl/fl mice and were further crossed with Cre-ERT2 mice for the generation of pmel-1 Cre-ERT2 Mybfl/fl mice. pmel-1 Cre-ERT2 Mybfl/fl mice were further crossed with Zeb2fl/fl mice to obtain pmel-1 Cre-ERT2 Mybfl/fl Zeb2wt/fl mice. Spleens from Tcf7GFP/+ mice51 were obtained from Avinash Bhandoola, National Cancer Institute and Hai-Hui Xue, Iowa University. Sex and age (6-10 weeks) matched mice were employed unless otherwise indicated.
Wild animals	No wild animals were used in the study.
Field-collected samples	No field-collected samples were employed in this study.
Ethics oversight	All mouse experiments were done with the approval of the National Cancer Institute Animal Care and Use Committee.

Note that full information on the approval of the study protocol must also be provided in the manuscript.

Flow Cytometry

Plots

Confirm that:

☒ The axis labels state the marker and fluorochrome used (e.g. CD4-FITC).

☒ The axis scales are clearly visible. Include numbers along axes only for bottom left plot of group (a 'group' is an analysis of identical markers).

☒ All plots are contour plots with outliers or pseudocolor plots.

☒ A numerical value for number of cells or percentage (with statistics) is provided.

Methodology

Sample preparation	Mice spleen and lymph nodes were homogenized using 40uM strainer and syringe. Lungs were homogenized using a gentleMACS™ Dissociator. Naive or whole CD8+ T cells were enriched using enrichment kits from Stem Cell technology.
Instrument	BD FACS Aria II, BD FACS LSRII, BD FACS Fortessa
Software	BD FACSDivaTM 8.0 was used to acquire the data, Flowjo_v9.9.4 was used to analyze the data
Cell population abundance	Purity after cell sort was determined by Flow Cytometry. The target population purity was higher than 88% for all experiments.
Gating strategy	All cell populations were analyzed by gating on lymphocytes, singlets, live cells and congenic/reporter markers (Thy1.1, Ly5.1, Ly5.2 or GFP depending on the markers expressed by the adoptively transferred cells).

☐ Tick this box to confirm that a figure exemplifying the gating strategy is provided in the Supplementary Information.